Author/s:
Zhao, W;Huang, Y;Siems, S;Manton, M

Title:
A characterization of clouds over the Great Barrier Reef and the role of local forcing

Date:
2022

Citation:
Zhao, W., Huang, Y., Siems, S. & Manton, M. (2022). A characterization of clouds over the Great Barrier Reef and the role of local forcing. International Journal of Climatology, 42 (12), pp.6647-6664. https://doi.org/10.1002/joc.7660.

Persistent Link:
https://hdl.handle.net/11343/301563

zhao wenhui (Orcid ID: 0000-0003-1947-8883)

A characterization of clouds over the Great Barrier Reef and the role of local forcing

Wenhui Zhao[1,3*], Yi Huang[2,3], Steven Siems[1,3], Michael Manton[1]

[1]School of Earth, Atmosphere and Environment, Monash University, Melbourne, VIC, Australia.

[2] School of Geography, Earth and Atmospheric Sciences, The University of Melbourne, Melbourne, VIC, Australia.

[3]Australian Research Council (ARC) Centre of Excellence for Climate Extreme (CLEX), Melbourne, VIC, Australia.

Corresponding author: Wenhui Zhao (wenhui.zhao@monash.edu)

Co-authors: Yi Huang (yi.huang4@unimelb.edu.au)

Steven Siems (steven.siems@monash.edu)

Michael Manton (michael.manton@monash.edu)

Key words: Great Barrier Reef, coral bleaching, cloud properties, orographic enhancement

We declare that this manuscript is original and has not been published elsewhere, nor is it currently under consideration for publication elsewhere. We have no conflicts of interest to disclose. As corresponding author, I confirm that the manuscript has been read and approved for submission by all the named authors.

This article has been accepted for publication and undergone full peer review but has not been through the copyediting, typesetting, pagination and proofreading process which may lead to differences between this version and the Version of Record. Please cite this article as doi: 10.1002/joc.7660

Abstract

A characterization of cloud properties associated with precipitation in the region around the Great Barrier Reef (GBR) is constructed using decade-long (2007-2017) satellite observations from Moderate Resolution Imaging Spectroradiometer (MODIS) and Cloud-Aerosol Lidar and Infrared Pathfinder Satellite Observations (CALIPSO) combined with CloudSat. The spatial and vertical distributions of low-level cloud properties over the region are also investigated and discussed. In general, different cloud types are observed over different regions and vary by season: high clouds are dominant over the low-latitudes in summer, altocumulus are mainly observed over north-east Queensland, and low-level clouds are dominant over the ocean and coast during the winter months at higher latitudes under a trade wind regime. A strong latitudinal dependence of total precipitation across the Greater GBR region is identified with a significant orographic enhancement near Cairns in the wet tropics. MODIS and CloudSat-CALIPSO cloud observations show good agreement on significant differences in low-level cloud microphysical properties between the land and the ocean. The largest land-ocean differences in warm cloud microphysical properties are found over the mid-latitudes near 18°S, which is strongly associated with orographic forcing, with these enhancements extending further east to the coral reef area. However, the frequency of warm cloud is not enhanced upwind of the mountains in the wet tropics. In addition, no significant differences in warm cloud properties between the actual GBR and the open ocean are identified. These results suggest that low-level clouds over the GBR do not show any significant response to the reef-related microphysical perturbations.

1 Introduction

As an important component of the Earth's climate system, clouds play a critical role in the global hydrological cycle and energy budget (Stephens., 2005). By interacting with radiation, clouds modulate the flow of energy through the atmosphere across a range of temporal and spatial scales. The important role of local cloud cover in modulating the regional energy budget across the Great Barrier Reef (GBR) was explored in Zhao et al. (2021), and the importance of clouds in preventing thermal coral bleaching was highlighted. Usually, warmer sea surface temperature (SST) is recognized as one of the main drivers of coral bleaching (Donner et al., 2005). Additionally, direct ultraviolet (UV) radiation is also implicated as a cause of coral stress, especially for tropical corals, including the GBR, that live in habitats where solar irradiance is extremely high (Lesser and Farrel, 2004; Shick et al., 1996). In this context, clouds have been suggested to temporally shade corals by limiting the UV radiation exposure and the sea surface heating caused by incoming solar radiation (Jones et al., 2017; Mumby et al., 2001). Zhao et al. (2021) identified a natural relationship between local cloud cover, radiation and SST, independent of the large-scale El Niño-Southern Oscillation (ENSO) impacts, particularly over the subtropical trade wind area where low clouds prevail. Low clouds reflect a significant fraction of incoming solar radiation and emit longwave radiation at relatively high temperatures, and thus exert a net cooling effect on the earth (Klein & Hartmann, 1993). Therefore, understanding the natural variability of cloud properties, especially low-level clouds, is essential to help understand the local atmosphere-ocean interactions across the GBR, a World Heritage site that spans over 2300 km off the coast of northeast Australia.

Shallow cloud systems are by their nature sensitive to perturbations in both their thermodynamic environment and microphysical background in which they exist (Stevens and Brenguier, 2009). The GBR contains the world's largest complex collection of coral reefs, and it has been suggested that the coral reef emissions of dimethylsulfide (DMS) may be an important contributor to the regional atmospheric aerosol loading that can serve as cloud condensation nuclei (CCN) (Cropp et al., 2018; Deschaseaux et al., 2016; Fischer and Jones 2012; Jones 2015). An enhanced production of CCN could,

potentially, affect the formation of low-level clouds such as cumulus and stratocumulus clouds and change the microphysics (e.g. effective radius and cloud droplet number concentration) of these clouds, changing their albedo, precipitation rate and lifetime (Jones et al., 2017; Lohmann and Feichter, 2005). On the other hand, variations in SST from the shallow water area off the coast to the deeper open ocean and from low to high latitudes over the GBR could also lead to differences in cloud properties across the region, given that the SST could significantly affect thermodynamic conditions of the circulation and consequently modify cloud properties such as cloud cover, cloud top height (Bony et al., 2004).

Located at the northeast coast of Australia, the marine atmospheric boundary layer cloud system over the GBR can also be influenced by a local-scale thermally driven sea-breeze circulation (Simpson, 1994; Li et al., 2009). A portion of the northeast Queensland coast along the GBR (near the town of Cairns; Figure 1) is known as the 'wet tropics' (e.g. Murphy et al. 2016), where the climatological south-easterly trade winds encounter orographic forcing. The highest elevation site in Queensland, Mt. Bartle Frere (elev. 1612 m), is located in this region with the Bellenden Ker Top station being one of the wettest stations in Australia receiving over 8000 mm of annual precipitation (Herwitz, 1986). It is, therefore, an open question as to whether this orographic forcing enhances cloud cover over the GBR, which in turn could locally protect corals from bleaching events.

The representation of shallow cumulus clouds in numerical weather prediction simulations is a long-standing challenge (e.g., Back and Bretherton 2009; Nam et al., 2012), with their smaller horizontal extent and broad range of time scales. However, satellite observations offer a unique possibility to survey cloud properties over a range of scales at different stages of their life cycle. The Moderate Resolution Imaging Spectroradiometer (MODIS) on the NASA Earth Observing System Terra and Aqua platforms provides unique measurements for deriving cloud properties (King et al., 1992, 2013). Cloud parameters derived from MODIS have been widely used for climate studies and model evaluations (Bennartz and Rausch, 2017; Kotarba, 2016; Suzuki et al., 2011; Wilcox et al., 2009). Information about the vertical distribution of clouds from

satellite observations has become available since 2006, when CloudSat (Stephens et al. 2002) and Cloud-Aerosol Lidar and Infrared Pathfinder Satellite Observations (CALIPSO) (Winker et al. 2007) joined the A-train satellite constellation. Given the advantages and limitations of different satellite observations, combining different satellite products and sensors would provide a more complete picture of the cloud properties across the region.

Considering the special location and its large extent of complex collection of coral reefs, the GBR is a unique natural laboratory to examine the sensitivity of low-level cloud properties in response to local forcing, including the regional aerosol loading and orography. In this study, we employ long-term satellite observations to characterize the macrophysical and microphysical properties of clouds over the GBR as well as the surrounding open ocean and coastal regions. In addition, we investigate the potential influence of local forcings on these properties and the implications for cloud cover and the protection of coral reefs. In particular, we seek to address two scientific questions: (1) What are the geographical and seasonal characteristics of clouds over the Greater GBR region? (2) Is there any evidence of variations in low-level cloud properties in response to local conditions, including the orographic forcing and the reef-related perturbations, across the region? The investigation is extended to examine precipitation across the domain, with a particular interest in the prevailing trade cumulus clouds. Addressing these questions will help to bridge the key knowledge gap in our understanding of the role of clouds over the GBR in the regional climate system, which is essential to help understand the local atmosphere-ocean interactions over the region. This knowledge may further aid the development of mitigation strategies for future mass coral bleaching events.

2 Data and Methods

2.1 Investigation area and study period

Our main study domain is (as in Zhao et al. 2021) shown in Figure 1, which is defined as the Greater GBR region. Three subdomains are defined in Figure 1a, namely land, GBR, and open ocean. Note that the most southern part of Papua New Guinea does not belong to the open ocean subdomain, and the western border of the open ocean is at 142.1° (shown by solid black line in Figure 1a). We chose the study period from 2007 to 2017. The 'wet tropics' is commonly defined to be located between roughly 15 and 19°S, along the coast near Cairns.

Figure 1. (a) Region 140 - 155°E, 10 - 25°S is the Greater GBR region referred to this study. Three subdomains are defined as land, GBR (where most of the coral reefs are located) and open ocean. **(b)** Bathymetric map of the domain. **(c)** Average number of footprint per granule in 1° latitude ×1° longitude grid box based on 2B-GEOPROF/2B-CLDCLASS-LIDAR_PDICD during the time period of 2007-2017 including daytime and nighttime. Note that grid boxes with no sample data are shaded in grey color. (a) and (b) are reproduced from Figure 1 in Zhao et al. (2021)

2.2 Datasets

2.2.1 CloudSat & CALIPSO cloud products

The CloudSat and CALIPSO (Cloud-Aerosol Lidar and Infrared Pathfinder Satellite Observation) satellites, parts of the sun-synchronous A-train constellation, were launched together in April 2006. The primary instrument on board CloudSat is the Cloud Profiling Radar (CPR), a 94 GHz radar with a 1.4 km wide effective footprint and 480m effective vertical resolution, which measures vertical structures of clouds and precipitation. It has the capacity to identify and penetrate optically thick clouds and detect small particles of liquid water and ice. Cloud-Aerosol Lidar with Orthogonal Polarization (CALIOP) is a spaceborne dual wavelength polarization lidar sensor on CALIPSO, which is designed to acquire vertical profiles of attenuated backscatter during both daytime and night-time. It can accurately detect most midlevel and high-level clouds which are often optically thin (e.g., altocumulus and cirrus clouds) (Wang and

Sassen, 2007; Deng et al., 2017). Therefore, combining lidar and radar measurements provides more reliable and detailed profiles of cloud properties (Sassen et al., 2009; Mace et al., 2009). The synergy of these active remote sensors along with other A-train sensors has provided near-simultaneous measurements that have been widely used for climate studies and model evaluations (Stephens et al., 2008; Li et al., 2011; Su et al., 2011; Huang et al., 2012, 2015).

Two of the daily orbits traverse our domain each day at the same local solar time with one overpass occurring during daytime (13:30 local time) and the other during nighttime (01:30 local time). It should be noted that CloudSat has been operating in a daylight-only mode because of a battery malfunction in 2011 (Stephens et al., 2017). Therefore, 4 years (2007-2010) of full data (including daytime and nighttime) and 7-yr (2011-2017) daytime-only observations have been applied to this study. CloudSat and CALIPSO are operating on a Sun-synchronous orbit with a mean equatorial altitude of 705 km and an inclination of 98.2 degrees (Stephens et al., 2008) (an example of the orbits that overpass the study domain in a year is shown in S1). The orbit is of constant size and shape and has a revisit time of 16 days. The footprint for a single profile is approximately 1.4km across-track by 1.8km along-track for CPR and around 1km by 1km for CALIOP, which result in the unevenly distributed measurements across the study domain with some grid boxes (1° latitude × 1° longitude) not covered at all (e.g. grey boxes in Fig. 1c) and large sample size differences possible between two adjacent grid boxes. Figure 1c illustrates the total number of footprints in each grid box (1° latitude ×1° longitude) and Table S1 shows the total number of footprints that pass through the Greater GBR region for the time period 2007-2017 separated into daytime and nighttime.

The level-2 cloud scenario classification product 2B-CLDCLASS-LIDAR (Sassen et al., 2008) provides a vertically resolved retrieval of cloud properties by synergistically combining CloudSat and CALIPSO observations at the CloudSat horizontal and vertical resolutions based on an optimal estimation framework. Clouds are grouped into cloud types (i.e. cirrus, altostratus, altocumulus, stratus, stratocumulus, cumulus, nimbostratus, and deep convection) using a detection algorithm (Wang and Sassen, 2007; Sassen and Wang, 2008), which categorizes the cloud type based on some basic

features (e.g., cloud base/top layer altitude, horizontal extent) of the major cloud types. Besides cloud layer type, the 2B-CLDCLASS-LIDAR data also provide other cloud layer information including cloud layer top and base height, cloud fraction and cloud phase.

Another CloudSat dataset employed in this study is the level-2B CloudSat Radar-Only Cloud Water Content Product (2B-CWC-RO). This product provides estimates of vertical profiles of cloud liquid and ice water content, effective radius, and related quantities for each radar profile measured by CloudSat's CPR. It should be noted that the 2B-CWC-RO product uses a temperature-dependent cloud water content (CWC) partition for clouds with temperature between 0°C and -20°C. Between these temperatures, the ice and liquid fractions are scaled linearly with temperature to obtain a profile that smoothly transitions from all ice at -20°C to all liquid at 0°C. Such a simple phase partition has been suggested to be problematic in several previous studies, due to the lack of physical basis. Therefore, in our study cloud microphysical properties are only examined for liquid (warm) clouds (cloud top temperature warmer than 0 °C) which primarily include cumulus and stratocumulus.

For the microphysical properties of cumulus and stratocumulus, we firstly identify the cloud type for each cloud layer from 2B-CLDCLASS-LIDAR. Then we re-grid each cloud layer to vertical bins at 500m intervals to accurately match the cloud type to microphysical properties for each layer using the cloud layer base and top altitudes for cumulus and stratocumulus. The vertical profiles of liquid cloud microphysical properties for cumulus and stratocumulus are then examined using the 2B-CWC-RO product at 500m vertical resolution.

2.2.2 Moderate Resolution Imaging Spectroradiometer (MODIS)

The National Aeronautics and Space Administration's (NASA) MODIS is an imaging instrument flown both on the Aqua and Terra platforms, which acquires data in 36 spectral bands with a spatial resolution of about 1km. In this study, the Level 2 Cloud Product (collection 6; Platnick et al. 2014) from the MODIS instrument onboard Aqua is employed to build a climatology of cloud microphysical properties at cloud top. The Level-2 Cloud Product provides retrievals of cloud fraction, cloud optical thickness, cloud

top temperature, and three droplet effective radius retrievals using near-infrared radiances observed at 1.6, 2.1, and 3.7 µm. From the retrieved cloud optical thickness and droplet effective radius, cloud droplet number concentration can be estimated (Brenguier et al., 2000). To be consistent with the analysis of CloudSat & CALIPSO, we calculate the cloud droplet number concentration (CDNC) for warm clouds only, which is identified based on cloud top temperature (warmer than 0°C) and cloud phase optical properties (liquid water), using the method given by Grosvenor and Wood (2014), which was modified from the original method in Bennartz (2007). The equation for calculating the CDNC is:

$$CDNC = \frac{2\sqrt{10}}{k\pi Q^3}\left[\frac{c_w cot}{\rho_l (r_{e,top})^5}\right]^{1/2} \quad (1)$$

where COT is cloud optical thickness, k is a factor related to the dispersion of the assumed cloud droplet size distribution; a constant value of 0.8 is adopted for k in this study. Similarly, Q is the scattering efficiency, which is set to its geometric optics limiting value of Q = 2. ρ_l is the liquid water density (1.0×10^3 kg m-3) and c_w is the temperature-dependent condensation rate (in kg m^{-4}), which is set to be 80% of its adiabatic value, as in Bennartz (2007). Note that the 80% adiabatic assumption may cause some temperature-dependent bias, but its contribution to the overall error budget is relatively small, as examined in Huang et al. (2016). r_e is the effective radius, which can be derived at different MODIS bands: 1.6, 2.1, and 3.7 μm. An important assumption made in equation (1) is that the retrieved effective radius is valid at the top of cloud, as indicated by the subscript 'top' in the above equation. However, satellite-derived effective radius is typically valid at some penetration depth below cloud top that depends on the observation wavelength and geometry (Bennartz and Rausch, 2017). The results from Bennartz and Rausch (2017) demonstrate that the penetration depth at 1.6 µm is about 2 to 3 times greater than that at 3.7 µm. Further detailed implications and limitations regarding this CDNC calculation is discussed in Bennartz and Rausch (2017). In this study, we use the effective radius retrieved at 3.7 µm to calculate the CDNC, as in Bennartz and Rausch (2017).

2.2.3 European Centre for Medium-Range Weather Forecasts (ECMWF) model analysis

The ECMWF-AUX dataset, produced by the CloudSat Data Processing Center, includes several meteorological ECMWF global variables which are mapped to the horizontal centre of each CloudSat profile and the vertical centre of each bin (CIRA, 2007). The temperature, specific humidity, and height fields at model pressure level from ECMWF-AUX analysis data are used in this study to calculate the lower troposphere stability (LTS) and estimated inversion strength (EIS) for selected profiles that are identified as cumulus and stratocumulus based on 2B-CLDCLASS-LIDAR product.

LTS is defined as the potential temperature (θ) difference between a nominal location in the free troposphere (typically 700hPa) and the surface:

$$LTS = \theta_{700} - \theta_{surface} \qquad (2)$$

The quantity EIS was developed to obtain a more precise estimate of the strength of the boundary layer inversion by removing the variability of the free tropospheric thermodynamic structure (Wood and Bretherton, 2006). EIS is defined as:

$$EIS = LTS - \Gamma_m^{850}(z_{700} - LCL) \quad (3)$$

Where Γ_m^{850} is the moist adiabatic potential temperature lapse rate, z_{700} is the altitude of the 700hPa pressure level, and LCL is the lifting condensation level computed using the expression LCL = 125 ($T - T_d$), which is based on the temperature (T) and dew point temperature (T_d) at the surface (Lawrence, 2005).

2.2.4 ERA5 reanalysis

ERA5 is the fifth-generation atmospheric reanalysis from the European Centre for Medium-Range Weather Forecasts (Hersbach et al., 2020). ERA5 uses the Integrated Forecasting System and includes atmosphere, land surface and ocean wave models. In this study, monthly total precipitation and wind field at 10 meters are derived from ERA5 with a resolution of 0.25° for the time period of 2007-2017.

3 Spatial-temporal characteristics of clouds over the Greater GBR region

3.1 Total cloud cover, wind and precipitation

The average total cloud cover (TCC) based on MODIS observations (2007-2017) shows significant latitudinal variation with strong land-ocean differences across the Greater GBR region (Figure 2a). High values of TCC are observed over the low-latitude ocean and most northern part of Queensland (Cape York), while southwest Queensland, furthest inland, experiences the least TCC throughout the year. The seasonality of TCC across the Greater GBR region is shown in Figure 2b-d. The maximum value of TCC is observed during the austral summer (DJF) over the deep tropics, as expected from the southward migration of the Intertropical Convergence Zone (ITCZ) during the tropical cyclone season from December to April. High values continue into the autumn months (MAM) during the retreat of the monsoon (Fig. 2d). The ITCZ migrates seasonally towards the warming hemisphere, with the southern branch over the western Pacific extending to 15°S, on average, during January-February-March season (Adam et al., 2016; Chen et al., 2008), which largely contributes to the enhanced cloudiness and precipitation across northern Australia in austral summer and autumn months (e.g. Murphy et al. 2016). The most significant land-ocean contrast in TCC is seen during the winter season (JJA), when western Queensland experiences the lowest TCC (less than 20%), while TCC of around 65% is observed over the ocean.

The trade wind regime is dominant over the GBR and open ocean during the winter season (e.g. Murphy 2017 and Fig. 5f-g). Accordingly, marine atmospheric boundary layer trade wind clouds largely contribute to the TCC over the open ocean in the winter months, while high clouds associated with the ITCZ, including the Madden-Julien Oscillation, and tropical cyclones are dominant during the summer month with the seasonal balance governed by the migration of the ITCZ. At higher latitudes, TCC inside the GBR is somewhat lower than in the outer open ocean (Fig. 2a). However, our analysis did not identify any significant difference in TCC at low latitudes when moving from the open ocean to the GBR. The most significant difference can be seen during winter (Fig.

2e), where around 35% TCC is observed inside the GBR, while the outer open ocean is experiencing TCC of 55%.

Figure 2. The averaged total cloud cover (TCC) over the Greater GBR region during the time period of 2007-2017 derived from MODIS observation. The three black triangles identify the towns of Cairns, Townville and Mackay, as per Figure 1.

To examine the vertical structure of these clouds, the cloud occurrence frequencies (COFs) of various cloud types are constructed using the 11-yr (2007-2017) CloudSat-CALIPSO data across the Greater GBR region. As shown in Fig. 3, the Greater GBR region is dominated by high clouds, altocumulus and low-level clouds. High clouds are mostly observed over the low-latitudes, and altocumulus tend to occur over land. Low-level clouds over the region are mostly observed over the ocean and along the north-east coastline of Queensland. Figure 4 shows significant variations in the annual cycle of the COF of high clouds and stratocumulus (Sc). There are more high clouds observed over the Greater GBR region during the austral warmer months (December - April), while the COF of stratocumulus peaks in austral winter time (June, July, August), which is consistent with the migration of the ITCZ, as previously discussed. The other types of clouds show little seasonal variation of COF, but there are slightly higher frequencies of altocumulus and cumulus (Cu) in October. We note that it is not possible to discern a diurnal cycle, including a sea breeze, in the cloud cover with A-train observations due to the sun-synchronous orbit. These observations, as a result, cannot provide evidence on complicated thermo-topographically induced diurnal oscillations (Lindesay and Tyson 1990).

Figure 3. 11-year (2007 -2017) averaged cloud occurrence frequency (COF) of eight cloud types over the Greater GBR region produced from CloudSat-CALIPSO data. White squares indicate no observations.

Figure 4. Annual cycle of cloud type COF over the Greater GBR region (140 - 155°E, 10 - 25°S, shown in Fig 1a) produced from CloudSat-CALIPSO data. Note that error bars represent +/- one standard deviation from the climatological mean.

Associated with the cloud climatology, the precipitation and wind fields over the Greater GBR region have also been examined. As Fig. 5a shows, there is a strong zonal dependence of total precipitation across the Greater GBR region, with a local maximum

associated with orography in the 'wet tropics' near Cairns (see Figure 1). A significant seasonal variation in total precipitation is also seen across the Greater GBR region with the peak occurring during austral summer (DJF), followed by the autumn months (MAM), as expected from the seasonal migration of the Australian summer monsoon and the ITCZ, where the prevailing south-easterly trade winds (Fig. 5f) are replaced by north-westerlies (Fig. 5h) at low-latitudes. As the tropical cyclone season also occurs during austral summer, it is possible that the increase in precipitation over the Greater GBR region during the warmer months is associated with deeper convective systems such as tropical cyclones and storms, as well as the background monsoon trough (Davidson et al., 2007; Moise et al., 2020). A slight increase in precipitation during summer is noted further south immediately along the coast down to the higher latitudes. As shown in Figure 1b, elevated terrain extends along the northeast coast of Australia. Under the south-easterly trade wind regime (Figure 5f), the mesoscale cloud systems over the Greater GBR region can be enhanced by upslope flow when they move from ocean over the orography. Thus, mountain ranges could alter the characteristics of cloud systems (e.g., Roe, 2005; Houze, 2012;), leading to enhanced precipitation over the windward slopes of mountains, where significant orographic effects on precipitation over Cairns can be noted during all seasons (Figure 5a-e), which makes it one of the wettest spots in Australia (Murphy et al. 2016).

The southeasterly trade wind regime that dominates the Greater GBR region has been noted in several studies (e.g. Wolanski, 1982). As shown in the 11-yr average wind field (Figure 5f), southeasterly winds prevail across GBR and open ocean. The strongest trade winds are found in winter (JJA), followed by spring and autumn with these months all clearly showing dominant southeasterly winds over the ocean. During the summer, with the migration of the ITCZ, the winds weaken and even reverse to a weak north to northwesterly wind at low latitudes (Figure 5h), while southeasterly winds keep prevailing in the southern part of the ocean. In all seasons we note a small weakening of the winds immediately upwind of the wet tropics presumably in response to orographic blocking.

Figure 5. (a) 11-yr (2007-2017) averaged monthly total precipitation derived from ERA5 over the Greater GBR region. **(b-e)** Seasonal variation of monthly total precipitation. **(f-j)** same as **(a-e)**, but for 10-m wind field derived from ERA5. Arrows show the direction of wind vector. Colour shading shows the wind speed at 10 m. Black triangles indicate the location of Cairns.

3.2 Low-level cloud properties and precipitation

The shallow convective clouds under the trade wind regime, commonly referred to as trade cumulus and stratocumulus, are directly connected to the underlying ocean. They are an important part of the overall climate system not only through their impact on the surface radiation budget and water budget, but also for their role in driving atmospheric circulations (Snodgrass et al., 2009; Vogel et al., 2016). It is of interest to investigate the variability of these shallow trade wind clouds specifically, across the GBR and open ocean, as well as their response to local forcings. We restrict this analysis to warm clouds only (cloud top temperatures warmer than 0°C and of liquid phase) as determined by MODIS observations (Platnick et al. 2017) and the Cu and Sc as observed by CloudSat (Figure 3).

As shown in Figure 6, there is a significant land-ocean difference in warm cloud properties, with warm clouds over the GBR and open ocean observed to have particles with larger effective radius (Re) (~15μm) but lower number concentration (less than 75 cm^{-3}) when compared to the land area. Warm cloud over the GBR and open ocean is observed to have small latitudinal variations in Re and CDNC, while larger variations in cloud properties are found over the land area, with CDNC decreasing and Re increasing from inland Queensland to the northeast coastline. These CDNC and Re gradients are likely a product of the coastal and orographic dynamics.

Figure 6: Warm cloud microphysical properties: (a) effective radius (Re) and (b) cloud droplet number concentration (CDNC) derived from MODIS observations at 3.7μm onboard Aqua (2007-2017).

Latitudinal variations of cloud top height (CTH) and precipitating cloud frequency for the Cu and Sc over the three sub-domains are examined by analyzing the data from CloudSat and CALIPSO (shown in Figure 7). Precipitating cloud is identified from the CPR radar reflectivity, where the criterion for drizzle of -15dBZe (profiles with maximum radar reflectivities larger than -15dBZe are considered to contain precipitating clouds) has

been applied. As such, the sampled clouds may be producing very light rain/drizzle that evaporates before reaching the surface. The results show that warm clouds (Cu + Sc) over land have higher tops than clouds over ocean, especially for Cu. The CTH for Cu over the land area peaks at high latitudes with a magnitude of 3km, while the maximum CTH over ocean is around 2km in the deep tropics. Sc is observed to have an approximately constant CTH across the Greater GBR region, regardless of latitude and sub-area. When considering precipitating cloud frequency for the two types of warm cloud, cumulus is found to have a tendency to precipitate over land, especially over mid- to high latitudes. In contrast, Sc is seen to precipitate more often over the ocean.

Figure 7. Latitudinal variations of the mean (solid lines) and standard deviation (shaded area) value of cloud top height of cumulus (top) and stratocumulus (bottom) over three sub-domains. Bar plot shows the frequency of precipitation for the two cloud types over three sub-domains. In both line and bar plot, green denotes land, blue denotes GBR and red denotes open ocean area.

Several studies have established relationships between LTS/EIS and low cloud amount to investigate the physical processes associated with boundary layer clouds (e.g., Klein and Hartmann, 1993; Wood and Hartmann, 2006). Here, we examine the LTS and EIS for Cu and Sc profiles that are identified by CloudSat by analysing the collocated ECWMF dataset. The result (Figure 8) shows that the mean values (2007-2017) of LTS and EIS for Cu over the ocean are both larger than that over land, which suggests that the Cu over land are associated with a less stable troposphere (low LTS/EIS) than that over the ocean, possibly explaining the more active Cu over land with higher CTH and a greater tendency to precipitate. In contrast, more fair-weather shallow cumulus develops over the ocean under a relatively stable tropospheric thermal environment, which leads to weaker precipitation rates. It should be noted that the limited timing of the CloudSat observations at 13.30 and 1.30 local time might also contribute to the observed LTS/EIS differences between land and ocean given the different timing in the diurnal cycle of convection over land and water (Tian, 2005; Yang and Slingo, 2001).

When turning to Sc, the mean LTS over the ocean is larger than that over land, which indicates that Sc developing over land is more likely to generate unstable convective precipitation. However, weaker differences in EIS could be seen for Sc over land and ocean, and drizzle is ubiquitous in marine boundary layer stratocumulus clouds with

much of it evaporating before reaching the surface (Wood et al., 2015; Zhou et al., 2015). Thus, we suspect that the Sc profiles associated with light drizzle, although under relatively more stable environmental conditions, contribute much to the high frequency of precipitating Sc over ocean, due to the longer lifetime of Sc compared with Cu cloud.

Figure 8. Statistics of lower troposphere stability (LTS) and estimated inversion strength (EIS) for Cu and Sc profiles, identified from CloudSat, over land and ocean. Variables used to calculate LTS and EIS are derived from collocated ECMWF dataset for the time period of 2007-2017.

4 The role of local forcing

4.1 Orographic enhancement of low-level cloud properties and precipitation

From the analysis of warm cloud microphysical properties (Figure 6), we see a significant extension of high values of Re from ocean to land near Cairns, which is likely to be highly associated with orographic impacts. Because the passive sensors of MODIS provide information only at cloud top, the analysis is extended to CloudSat & CALIPSO profile data, which allows us to examine vertical profiles of cloud properties. Given that the tops of warm clouds tend to be below 3000m (Figure 7) and that CloudSat measurements within the lowest 750 m are affected by ground clutter (Mace et al., 2007; Marchand et al., 2008), we limit our analysis to warm cloud profiles of Cu and Sc between 750 and 3000 m.

The vertical distributions of liquid cloud microphysical properties, including liquid water content (LWC), Re and CDNC of liquid particles have been examined based on CloudSat-CALIPSO data for land area and ocean area (including GBR and open ocean) (shown in Figure 9). We note that the land area is geographical diverse ranging from the rainforests along the coast to the dry in-land regions of southwestern Queensland. As our analysis only considers the warm clouds, the 'land' region is heavily weighted towards warm clouds over the coast and near-coastal orographic regions. The differences of cloud properties between land area and ocean area are shown in Figure 9c, f & i. To test the significance of the differences, we use the two-sample t-test method and the results presented below are statistically significant at the 95% confidence level.

Figure 9. Zonally averaged vertical distribution of LWC of low-level clouds over (a) land area and (b) ocean area (GBR + open ocean) and (c) difference between (a) and (b). (d-f) as in (a-c),

but for Re of liquid particles. (g-i) same as (a-c), but for CDNC of liquid particles. The significance of the difference has been tested using the two-sample t-test method, and note that all results presented above are statistically significant at the 95% confidence level.

Focusing first on the distribution of CDNC of warm cloud liquid particles over land and ocean area (Figure 9g-h), we see very similar patterns, with CDNC ranging from 85/cm^3 at 750 m to 60/cm^3 at 3km altitude level with little variation from low latitudes to high latitudes. There are significant positive differences in CDNC of warm clouds (Figure 9i) between the land and ocean from low-latitudes to high-latitudes at all altitudes, which is consistent with the analysis of Figure 6b. This expected land-ocean positive difference in CDNC is likely associated with terrestrial aerosol loading, where high concentration of anthropogenic aerosols (e.g. from urban pollution and industrial activity) and other continental aerosols (e.g. dust) could serve as CCN which leads to enhanced droplet number concentration over land.

The climatological values of Re and LWC of warm clouds over the ocean area decrease smoothly with altitude with no significant latitudinal variations (Figure 9b & e). On the other hand, the zonal vertical distributions of Re and LWC over land show marked variations with latitude, where the most significant positive land-ocean differences are both located near 18°S in the wet tropics (Figure 9c & f). It is likely that the high value of LWC and Re over land at 18°S is associated with the orographic impacts on precipitation as discussed previously (see Figure 5 and 7). However, orographic precipitation depends on many parameters, such as the terrain features, atmospheric stability (which is discussed later) and upslope velocity (Roe, 2005; Houze, 2012; Kunz and Wassermann, 2011). Further analysis of the mountain cloud-precipitation system over the Greater GBR region through in-situ observations and numerical simulations is necessary to elucidate the detailed processes involved. Nevertheless, our analysis demonstrates that low-level cloud properties over the Greater GBR region show strong response to the orographic forcing at mid-tropics near Cairns in the wet tropics. These results could serve as background knowledge of the orographic enhancement on clouds and precipitation, which helps better understanding of the local cloud-precipitation system over the Greater GBR region.

Given the noted significant orographic enhancement around 18°S in the wet tropics, it is of interest to examine how far east this enhancement of cloud properties extends when considering the potential natural shading of corals by clouds, which then could protect corals from coral bleaching events. To this end, the cross-sectional distribution of warm cloud properties over a band around 18°S band (the wet tropics) is further explored in Figure 10b-d. It should be noted that these features of low-level clouds are found to be statistically significant using a method described by Lancaster (1961), and detailed results can be found in the Figure S2. A significant variation in cloud properties associated with orography can be seen, where large values of LWC and Re are observed over land. As shown in Figure 10b-c, low-level clouds at the windward side of the mountains have large LWC with relatively large Re, especially at low altitudes. This significant enhancement, including LWC and Re, extends further east to the coral reef area (shown by dashed lines) (Fig. 10e-g), which is likely to lead to enhanced cloud reflectance that could potentially protect corals in this area from direct radiation exposure. Although the magnitude of this enhancement is relatively small (~0.5×100mg/cm^3 and ~1μm) compared to the climatological mean values (~9×100mg/cm^3 and ~20μm), the positive differences that reach up to 2.5km height are statistically significant according to the two-sample t-test method. This enhancement has been further tested by examining another latitude band (centered at 15°S) that does not intercept areas with topography (see Figure S3). For this relatively flat coastline, no significant enhancement has been found to be extending further east over the GBR area.

When looking at the total cloud cover distribution observed by MODIS (Figure 2), there is a slight increase in TCC over the wet tropics during winter months, when the trade winds are strongest (Figure 5j). However, there is little to no significant TCC enhancement around the wet tropics identified during the warmer (coral bleaching) season. It is noted that the TCC derived from MODIS accounts for all cloud types, in which high-level clouds may be prominent and where TCC is highly influenced by tropical cyclones and southward migration of the ITCZ rather than by local orographic enhancement in Austral summer months. From CloudSat observations, our result (Figure 3) shows some enhancement of Sc COF over the orography in the wet tropics,

but this enhancement does not extend further east to the coral reef area. On the other hand, small COF enhancement of altocumulus is observed upwind of the mountains near the wet tropics, but these results may be biased by the limited spatial and temporal resolution of the sun-synchronous satellite observations. In this context, analysis of high-resolution observations would be needed to address the open question of cloud cover enhancement over the wet tropics upwind of the mountains.

Figure 10. (a) Bathymetric map of the Greater GBR region with red lines indicating the 18°S latitude band. (b-d) 18°S latitude-band cross-section distribution of cloud microphysical properties (LWC, Re and CDNC of liquid particles). Dashed lines denote the location of the coral reef (GBR area). Note that all results shown above are statistically significant at 95% confidence level. (e-g) Difference plots between the GBR and limited open ocean (same width as the GBR, shown by blue dashed lines) at the 18°S latitude-band for each altitude level same as (b-d). The black dots indicate the differences that are statistically significant at the 95% significant level.

4.2 Potential responses of cloud properties to coral reef emissions

A small but consistent difference in TCC between open ocean and GBR (Figure 2) has been identified over higher latitudes, where there is a large collection of coral reefs. When considering the hypothesis that clouds and precipitation may be modulated by biogenic emissions associated with coral reefs (Cropp et al., 2018; Fischer and Jones 2012), it is of interest to examine variations of cloud properties that may be linked to the transition from open ocean to GBR. It is interesting to note that the most significant difference in TCC between GBR and outer open ocean at higher latitudes is observed during winter (Fig. 2e), when the biogenic emission of coral reef is considered to be low because of the lack of environmental stresses, such as extreme warm sea surface temperatures (Charlson et al. 1987). On the other hand, the variation in SST from GBR to the open ocean through marine atmospheric boundary layer processes, especially at higher latitudes in winter (see Figure S4), may affect cloud properties, especially low-level clouds (Qu et al., 2015; Takahashi et al., 2021). It should be noted that the TCC (Figure 2) derived from MODIS is a consideration of all cloud types, in which high-level clouds may be prominent, especially over the deep tropics. However, low-level clouds play an important role in air-sea interaction processes, where low-level clouds properties show strong sensitivity to the surface conditions (Klein et al. 2017). Thus, low-

level clouds should be at first place to consider when addressing the reef-emissions hypothesis.

From Figures 3 and 7, we see that the COF and precipitation frequency of low-level clouds (Sc+Cu) over the GBR, where there are many coral reefs, are very similar to those over the open ocean. In other words, our analysis does not identify clear evidence of a response of low-level cloud macro-physical properties to coral reef related local forcing. Not surprisingly, analysis of the warm cloud microphysical properties (Figure 6) shows a significant land-ocean contrast across the Greater GBR region, but no significant difference is noted between the GBR and open ocean. This is consistent with the vertical distribution analysis based on CloudSat and CALIPSO (Figure 11), where the profiles of LWC, Re and CDNC of liquid particles for GBR and open ocean are nearly the same at all altitudes. In summary, our statistical analysis of independent satellite datasets consistently finds no evidence of significant differences in low-level cloud microphysical properties between open ocean and GBR.

Figure 11. (a) Vertical profile of liquid water content (LWC), (b) Re of liquid particles and (c) CDNC of liquid particles of low-level clouds (stratocumulus + cumulus) over GBR (blue lines) and open ocean (red lines). Solid lines represent average values at each altitude, and shading indicates the standard deviation.

When considering the dominant south-easterly trade wind regime over the open ocean and GBR (Figure 5f), we select two sub-domains A (A1 and A2) and B along the wind direction to further explore any potential variations in cloud properties (Figure 12a) in a Lagrangian framework. Subdomain B is at a downwind location just before the main flow moves over the land area near Cairns. A1 and A2 are at upwind locations inside and outside of the coral reef area (black line in the Figure 12a). Microphysical properties of warm clouds derived from CloudSat and CALIPSO are examined for each sub-area (Figure 12b). Once again, no significant difference is noted in the cloud microphysical properties of warm clouds between subdomain A (including A1 and A2) and B at all altitudes.

Cropp et al. (2018) suggested that the GBR may be a significant source of marine aerosol emissions and could potentially influence the atmosphere above them. However, they

do not influence the coral's local environment during windy period, as the products are transported and dispersed by the wind. On the other hand, a climate model simulation by Fiddes et al, (2021) showed a small response of the number concentration of particles greater than 3nm dry diameter (N_3) and CCN to the DMS perturbations over the Maritime Continent-Australian region, with nearly zero differences in N_3 and CCN when coral reef DMS emissions are removed. Our findings are essentially consistent with the results from these previous studies, although our analysis has focused on identifying any observable footprints that coral reef emissions might have left on clouds over the GBR, rather than on examining the aerosol themselves. We recognise that the complex interactions between regional marine biogenic emissions and meteorological factors covering a range of scales requires carefully analysis. For example, the scavenging effects of precipitation can lead to the removal of aerosol particles, which limits the detection of aerosol effects on clouds. Nevertheless, our study indicates that there are no significant changes in warm cloud properties between the coral reef area and outer reef-free ocean as observed by independent satellites. It is expected that this observation will aid further analyses of the local cloud-climate interactions over the Greater GBR region related to the protection of the coral reefs.

Figure 12. (a) Climatology of wind field at 10m derived from ERA5 for the period of 2007-2017. Three red boxes show the locations of three target subdomains A1, A2 and B. **(b)** Vertical profiles of LWC, Re and CDNC of low-level clouds over sub-domain A1, A2 and B derived from CloudSat & CALIPSO.

5 Conclusions

In this study, we employed decade-long (2007-2017) satellite datasets from MODIS and CloudSat & CALIPSO and reanalysis datasets from ERA5 to characterize the cloud properties and the associated precipitation over the Greater GBR region. The atmospheric stability associated with low-level cloud properties and the role of local forcings are also investigated and discussed. The main findings of this study are summarized as follows:

1. In general, the Greater GBR region is found to be mainly dominated by high cloud, altocumulus and low-level cloud types (cumulus and stratocumulus). Strong geographical and seasonal variabilities are noted, with high clouds dominant over low latitudes in summer, altocumulus mainly observed over north-east Queensland, and low-level clouds covering most of the water area and the land along the coast during winter months. The seasonality is primarily driven by the seasonal migration of the ITCZ.

2. Our analysis reveals a strong latitudinal dependence of total precipitation across the Greater GBR region and a significant precipitation enhancement associated with orography near Cairns. The prevailing southeasterly trade wind largely controls the boundary layer of the GBR and the open ocean which also varies seasonally in alignment with the ITCZ.

3. Cumulus cloud over land area tends to have higher cloud tops and to precipitate more often, under relatively unstable lower troposphere condition, than those over the water area (GBR and open ocean). On the other hand, stratocumulus precipitates more often over the ocean, with possibly light drizzle. The cloud top height of stratocumulus does not vary with latitude and from ocean to land.

4. Significant differences in cloud properties of warm clouds are found between the land and water areas, with the largest land-ocean differences in Re and LWC over the mid-tropics near 18°S (the wet tropics), which is likely associated with orographic forcing. This orographic enhancement is observed to extend further

east to the coral reef area, which may protect corals through larger cloud reflectance; however, there is no significant low cloud COF enhancement extending upwind of the mountains.

5. Our analysis did not identify any significant difference in warm cloud properties between GBR and open ocean. Similarly, no clear differences in cloud properties at upwind and downwind sites within the coral reef region along the dominant trade wind direction are found in the analysis. These results suggest that low-level cloud over the Greater GBR region does not show any significant response to the reef-related microphysical perturbations.

While we characterized cloud properties based on long-term satellite observations, which provide background information on the nature and variability of cloud across the Greater GBR region, it is recognised that higher temporal resolution, e.g. diurnal cycle of these low-level clouds, including a sea breeze, should also be investigated. Low-level cloud development is well-known to show strong responses to the day-night cycle of solar flux. During daytime, strong solar heating of the surface could drive convection and generate cumuliform clouds, while at night stratiform clouds are more likely to form because of the boundary layer cooling condensation. Maritime convection can also be enhanced during nighttime by cloud-top cooling relative to nearby clear areas. A fundamental difference in the convective life cycle between land and ocean has been suggested in terms of peaking time, precipitation type and intensity (Futyan and Del Genio, 2007; Matsui et al., 2016). As such, it is important to take the diurnal cycle into account to avoid biases. Given the limitation of the polar orbiting satellite observations that we have applied in this study, observations with higher spatial and temporal resolution will be necessary to investigate the full lifecycle of these clouds and the development of onshore precipitation.

It is worth noting that a primary objective of this study has been to identify any observable changes of low-level cloud properties over the Greater GBR region that might be related to the impacts of biogenetic emissions or orographic forcing. Future work needs to be focused on detailing the key physical mechanisms and processes

involved. In particular, analysis of the thermal-dynamical mechanisms that relate to these shallow clouds is needed using high-resolution numerical simulations and observational data. Nevertheless, our analysis shed some light on the understanding of the nature and variability of clouds over the Greater GBR region, where the role of clouds in thermal coral bleaching events have only recently been identified. This research also helps determine future research priorities on advancing the understanding of cloud-climate interactions and the hydrological cycle over this climatically important region.

References

Adam, Ori, Bischoff, Tobias, & Schneider, Tapio. (2016) Seasonal and Interannual Variations of the Energy Flux Equator and ITCZ. Part I. Journal of Climate, 29(9), 3219–3230. https://doi.org/10.1175/JCLI-D-15-0512.1

Back, Larissa E, & Bretherton, Christopher S. (2009) A Simple Model of Climatological Rainfall and Vertical Motion Patterns over the Tropical Oceans. Journal of Climate, 22(23), 6477–6497. https://doi.org/10.1175/2009JCLI2393.1

Bennartz, R., (2007) Global assessment of marine boundary layer cloud droplet number concentration from satellite. J. Geophys. Res., 112, D02201, doi:10.1029/2006JD007547.

Bennartz, Ralf, & Rausch, John. (2017) Global and regional estimates of warm cloud droplet number concentration based on 13 years of AQUA-MODIS observations. Atmospheric Chemistry and Physics, 17(16), 9815–9836. https://doi.org/10.5194/acp-17-9815-2017

Bony, S., Dufresne, J.-L., Le Treut, H., Morcrette, J.-J. and Senior, C. (2004) On dynamic and thermodynamic components of cloud changes. Climate Dynamics, 22(2–3), 71–86. https://doi.org/10.1007/s00382-003-0369-6.

Brenguier, J. L., Pawlowska, H., Schuller, L., Preusker, R., Fischer, J., and Fouquart, Y. (2000) Radiative properties of boundary layer clouds: Droplet effective radius versus number concentration, J. Atmos. Sci., 57, 803–821.

Chen, Baode, Lin, Xin, & Bacmeister, Julio T. (2008) Frequency Distribution of Daily ITCZ Patterns over the Western–Central Pacific. Journal of Climate, 21(17), 4207–4222. https://doi.org/10.1175/2008JCLI1973.1

Charlson, R. J., Lovelock, J. E., Andreae, M. O., and Warren, S. G. (1987) Oceanic phytoplankton, atmospheric sulphur, cloud albedo and climate, Nature, 326, 655–661, https://doi.org/10.1038/326655a0.

CIRA (Cooperative Institute for Research in the Atmosphere) (2007) CloudSat project: A NASA Earth System Science Pathfinder Mission: CloudSat standard data products handbook. Fort Collins, CO 80523. Retrieved from http://www.cloudsat.cira.colostate.edu/cloudsat_documentation/CloudSat_Data_Users_Handbook.pdf

Cropp, Roger, Gabric, Albert, van Tran, Dien, Jones, Graham, Swan, Hilton, & Butler, Harry. (2018) Coral reef aerosol emissions in response to irradiance stress in the Great Barrier Reef, Australia. Ambio, 47(6), 671–681. https://doi.org/10.1007/s13280-018-1018-y

Davidson, N.E., Tory, K.J., Reeder, M.J. and Drosdowsky, W.L. (2007) Extratropical–tropical interaction during onset of the Australian monsoon: reanalysis diagnostics and idealized dry 2326 MOISE ET AL. simulations. Journal of the Atmospheric Sciences, 64, 3475–3498. https://doi.org/10.1175/JAS4034.1.

Deng, H., Pepin, N. and Chen, Y. (2017) Changes of snowfall under warming in the Tibetan plateau. Journal of Geophysical Research: Atmospheres, 122, 7323–7341.

Deschaseaux, E., E. Deschaseaux, G. Jones, and H. Swan. (2016) Dimethylated sulfur compounds in coral-reef ecosystems. Environmental Chemistry 13: 239–251. https://doi.org/10.1071/ en14258.

Donner, S. D., Skirving, W. J., Little, C. M., Oppenheimer, M., & Hoegh-Guldberg, O. (2005) Global assessment of coral bleaching and required rates of adaptation under climate change. Global Change Biology. 11, 2251–2265. https://doi.org/10.1111/j.1365-2486.2005.01073.x

Fiddes, Sonya L, Woodhouse, Matthew T, Lane, Todd P, & Schofield, Robyn. (2021) Coral-reef-derived dimethyl sulfide and the climatic impact of the loss of coral reefs. Atmospheric Chemistry and Physics, 21(8), 5883–5903. https://doi.org/10.5194/acp-21-5883-2021

Fischer, E., and G. Jones. (2012) Atmospheric dimethylsulphide production from corals in the Great Barrier Reef and links to solar radiation, climate and coral bleaching. Biogeochemistry 110: 31–46.

Futyan, J. M., & Del Genio, A. D. (2007) Deep Convective System Evolution over Africa and the Tropical Atlantic, *Journal of Climate*, *20*(20), 5041-5060.

Grosvenor, D. P., and R. Wood, (2014) On the effect of solar zenith angle on MODIS cloud optical and microphysical retrievals. Atmos. Chem. Phys., 14, 7291–7321, doi:10.5194/acp-14-7291-2014.

Hersbach, H., Bell, B., Berrisford, P., Hirahara, S., Horányi, A., Muñoz-Sabater, J., Nicolas, J., Peubey, C., Radu, R., Schepers, D., Simmons, A., Soci, C., Abdalla, S., Abellan, X., Balsamo, G., Bechtold, P., Biavati, G., Bidlot, J., Bonavita, M., De Chiara, G., Dahlgren, P., Dee, D., Diamantakis, M., Dragani, R., Flemming, J., Forbes, R., Fuentes, M., Geer, A., Haimberger, L., Healy, S., Hogan, R.J., Hólm, E., Janisková, M., Keeley, S., Laloyaux, P., Lopez, P., Lupu, C., Radnoti, G., de Rosnay, P., Rozum, I., Vamborg, F., Villaume, S. and Thépaut, J.-N. (2020) The ERA5 global reanalysis. Quarterly Journal of the Royal Meteorological Society, 146(730), 1999–2049

Herwitz, Stanley R. (1986) Infiltration-excess caused by Stemflow in a cyclone-prone tropical rainforest. Earth Surface Processes and Landforms, 11(4), 401–412. https://doi.org/10.1002/esp.3290110406

Houze, R.A., (2012) Orographic effects on precipitating clouds. Rev. Geophys. 50https://doi.org/10.1029/2011RG000365. RG1001, 47pp.

Huang, Yi, Siems, Steven T, Manton, Michael J, Hande, Luke B, & Haynes, John M. (2012) The structure of low-altitude clouds over the Southern Ocean as seen by CloudSat. Journal of Climate, 25(7), 2535–2546. https://doi.org/10.1175/JCLI-D-11-00131.1

Huang, Y., Protat, A., Siems, S. T., & Manton, M. J. (2015) A-Train Observations of Maritime Midlatitude Storm-Track Cloud Systems: Comparing the Southern Ocean against the North Atlantic, Journal of Climate, 28(5), 1920-1939. Retrieved Apr 18, 2021, from https://journals.ametsoc.org/view/journals/clim/28/5/jcli-d-14-00169.1.xml

Huang, Yi, Siems, Steven T, Manton, Michael J, Rosenfeld, Daniel, Marchand, Roger, McFarquhar, Greg M, & Protat, Alain. (2016) What is the Role of Sea Surface Temperature in Modulating Cloud and Precipitation Properties over the Southern Ocean? Journal of Climate, 29(20), 7453–7476. https://doi.org/10.1175/JCLI-D-15-0768.1

Jones, G.B. (2015) The reef sulphur cycle: Influence on climate and ecosystem services. In Ethnobiology of corals and coral reefs, ed. N.E. Narchi, and L.L. Price, 27–57. Cham: Springer.

Jones, G., Curran, M., Swan, H. and Deschaseaux, E. (2017) Dimethylsulfide and Coral Bleaching: Links to Solar Radiation, Low Level Cloud and the Regulation of Seawater Temperatures and Climate in the Great Barrier Reef. American Journal of Climate Change, 6, 328-359. doi: 10.4236/ajcc.2017.62017.

King, M. D., Y. J. Kaufman, W. P. Menzel, and D. Tanre (1992) Remote sensing of cloud, aerosol and water vapor properties from the moderate resolution imaging spectrometer (MODIS), IEEE Trans. Geosci. Remote Sens., 30, 2–27

King, M. D., S. Platnick, W. P. Menzel, S. A. Ackerman, and P. A. Hubanks (2013) Spatial and temporal distribution of clouds observed by MODIS onboard the Terra and Aqua satellites, IEEE Trans. Geosci. Remote Sens., 51, 3826–3852.

Klein, S. A. and D. L. Hartmann (1993) The seasonal cycle of low stratiform clouds. J. Climate, 6, 1588-1606.

Klein, S. A., A. Hall, J. R. Norris, and R. Pincus, (2017) Low-cloud feedbacksfrom cloud-controlling factors: A review.Surv. Geophys.,38,1307–1329,https://doi.org/10.1007/s10712-017-9433-3.

Kotarba, Andrzej Z. (2016) Regional high-resolution cloud climatology based on MODIS cloud detection data. International Journal of Climatology, 36(8), 3105–3115. https://doi.org/10.1002/joc.4539

Kunz, M., Wassermann, S., (2011) Sensitivity of flow dynamics and orographic precipitation to changing ambient conditions in idealised model simulations. Meteorol. G. Choudhury, et al. Atmospheric Environment 214 (2019) 11683117Z. 20 (2), 199–215.

Lancaster, H. O. (1961) Significance tests in discrete distribution, Journal of the American Statistical Association, 56, 223-234.

Lawrence, M. G. (2005) The relationship between relative humidity and the dewpoint temperature in moist air: A simple conversion and applications, Bull. Am. Meteorol. Soc., 86, 225–233, doi:10.1175/BAMS-86- 2-225.

Lesser, M. P., & Farrell, J. H. (2004) Exposure to solar radiation increases damage to both host tissues and algal symbionts of corals during thermal stress. Coral Reefs, 23, 367– 377

Lohmann, U, & Feichter, J. (2005) Global indirect aerosol effects: A review. Atmospheric Chemistry and Physics, 5(3), 715–737. https://doi.org/10.5194/acp-5-715-2005

Li, J. F., D. E. Waliser, and J. H. Jiang (2011) Correction to "Comparisons of satellites liquid water estimates to ECMWF and GMAO analyses, 20th century IPCC AR4 climate simulations, and GCM simulations", Geophys. Res. Lett., 38, L24807, doi:10.1029/2011GL049956

Li, Xiaofeng, Zheng, Weizhong, Pichel, W. G, Zou, Cheng-Zhi, Clemente-Colón, P, & Maturi, E. (2009) Multisatellite observations and numerical simulation of an along-coast cumulus cloud line induced by sea-breeze circulation. International Journal of Remote Sensing, 30(14), 3573–3584. https://doi.org/10.1080/01431160802585330

Lindesay, J. A, & Tyson, P. D. (1990) Thermo-topographically induced boundary layer oscillations over the central Namib, southern Africa. International Journal of Climatology, 10(1), 63–77. https://doi.org/10.1002/joc.3370100108

Mace, G. G., Q. Zhang, M. Vaughan, R. Marchand, G. Stephens, C. Trepte, and D. Winker (2009) A description of hydrometeor layer occurrence statistics derived from the first year of merged CloudSat and CALIPSO data, J. Geophys. Res., 114, D00A26, doi:10.1029/2007JD009755.

Mace, G. G., R. Marchand, Q. Zhang, and G. Stephens (2007) Global hydrometeor occurrence as observed by CloudSat: Initial observations from summer 2006, Geophys. Res. Lett., 34, L09808, doi:10.1029/2006GL029017

Marchand, R. T., G. G. Mace, T. P. Ackerman, and G. Stephens, (2008) Hydrometeor detection usingCloudSat—An Earth or-biting 94-GHz cloud radar.J. Atmos. Oceanic Technol.,25,519–533, doi:10.1175/2007JTECHA1006.1.

Matsui, T., Chern, J., Tao, W., Lang, S., Satoh, M., Hashino, T., & Kubota, T. (2016) On the Land–Ocean Contrast of Tropical Convection and Microphysics Statistics Derived from TRMM Satellite Signals and Global Storm-Resolving Models, *Journal of Hydrometeorology*, *17*(5), 1425-1445.

Moise, Aurel, Smith, Ian, Brown, Josephine R, Colman, Robert, & Narsey, Sugata. (2020) Observed and projected intra-seasonal variability of Australian monsoon rainfall. International Journal of Climatology, 40(4), 2310–2327. https://doi.org/10.1002/joc.6334

Mumby, P., Chisholm, J., Edwards, A., Andrefouet, S., & Jaubert, J. (2001) Cloudy weather may have saved Society Island reef corals during the 1998 ENSO event, Marine Ecology Progress Series, 222, 209–216, https://doi.org/10.3354/meps222209

Murphy, M. J., Jr., Siems, S. T., & Manton, M. J. (2016) Regional Variation in the Wet Season of Northern Australia, *Monthly Weather Review*, *144*(12), 4941-4962. Retrieved Sep 2, 2021, from https://journals.ametsoc.org/view/journals/mwre/144/12/mwr-d-16-0133.1.xml

Murphy, Michael James. (2017) Variability in the trade wind regime and wet season of Northeastern Queensland.

Nam, C., Bony, S., Dufresne, J.-L., & Chepfer, H. (2012) The 'too few, too bright' tropical low-cloud problem in CMIP5 models. Geophysical Research Letters, 39, L21801. https://doi.org/10.1029/2012GL053421

Platnick, S., and Coauthors, (2014) MODIS Cloud Optical Properties: User Guide for the Collection 6 Level-2 MOD06/MYD06 product and associated level-3 datasets. NASA Goddard Space Flight Center, 140 pp.

Platnick, S., K. G. Meyer, M. D. King, G. Wind, N. Amarasinghe, B. Marchant, G. T. Arnold, Z. Zhang, P. A. Hubanks, R. E. Holz, P. Yang, W. L. Ridgway, and J. Riedi, (2017) The MODIS cloud optical and microphysical products: Collection 6 updates and examples from Terra and Aqua. IEEE Trans. Geosci. Remote Sens., 55, 502-525.

Qu X, Hall A, Klein SA, DeAngelis AM (2015) Positive tropical marine low-cloud cover feedback inferred from cloud-controlling factors. Geophys Res Lett 42:7767–7775. https://doi. org/10.1002/2015GL065627

Roe, G.H., (2005) Orographic precipitation. Annu. Rev. Earth Planet. Sci. 33, 645–671. https://doi.org/10.1146/annurev.earth.33.092203.122541.

Sassen, K., and Z. Wang (2008) Classifying clouds around the globe with the CloudSat radar: 1-year of results, Geophys. Res. Lett., 35, L04805, doi:10.1029/2007GL032591.

Sassen, K., Z. Wang, and D. Liu, (2008) Global distribution of cirrus clouds from CloudSat/Cloud-Aerosol Lidar and Infrared Pathfinder Satellite Observations (CALIPSO) measurements, J. Geophys. Res., 113, D00A12, doi:10.1029/2008JD009972.

Sassen, K., Z. Wang, and D. Liu (2009) Cirrus clouds and deep convection in the tropics: Insights from CALIPSO and CloudSat, J. Geophys. Res., 114, D00H06, doi:10.1029/2009JD011916.

Shick, J. M., M. P. Lesser, and P. L. Jokiel. (1996) Effects of ultraviolet radiation on corals and other coral reef organisms. Glob. Change Biol. 2: 527–545

Simpson, J.E., (1994) Sea Breeze and Local Winds (Cambridge, UK: Cambridge University Press).

Snodgrass, E. R., Di Girolamo, L., & Rauber, R. M. (2009) Precipitation Characteristics of Trade Wind Clouds during RICO Derived from Radar, Satellite, and Aircraft Measurements, *Journal of Applied Meteorology and Climatology*, *48*(3), 464-483. Retrieved Jul 4, 2021, from https://journals.ametsoc.org/view/journals/apme/48/3/2008jamc1946.1.xml

Stephens, G. L., D. G. Vane, R. J. Boain et al. (2002) The CloudSat Mission and the A-Train: A new dimension of space-based observations of clouds and precipitation, Bull. Am. Meteorol. Soc., 83, 1771-1790.

Stephens G. L. (2005) Cloud feedbacks in the climate system: a critical review. J Clim 18, 237–273. 33. https://doi.org/10.1175/JCLI-3243.1

Stephens, G., Winker, D., Pelon, J., Trepte, C., Vane, D., Yuhas, C., et al. (2017) CloudSat and CALIPSO within the A-Train: Ten years of actively observing the Earth system. Bulletin of the American Meteorological Society, 99, 569–581. https://doi.org/10.1175/BAMS-D-16- 0324.1

Stephens, G. L., et al. (2008) CloudSat mission: Performance and early science after the first year of operation, J. Geophys. Res., 113, D00A18, doi:10.1029/2008JD009982

Stevens B and Brenguier J-L (2009) Cloud-controlling factors: low clouds Clouds in the Perturbed Climate System: Their Relationship to Energy Balance, Atmospheric Dynamics, and Precipitation ed J Heintzenberg and R J Charlson (Cambridge, MA: MIT Press) pp 173–96

Su, H., et al. (2011) Comparison of regime-sorted tropical cloud profiles observed by CloudSat with GEOS5 analyses and two general circulation model simulations, J. Geophys. Res., 116, D09104, doi:10.1029/2010JD014971.

Suzuki, K., Stephens, G. L., van den Heever, S. C., and Nakajima, T. Y. (2011) Diagnosis of the Warm Rain Process in CloudResolving Models Using Joint CloudSat and MODIS Observations, J. Atmos. Sci., 68, 2655–2670, https://doi.org/10.1175/jasd-10-05026.1.

Takahashi, Naoya, Hayasaka, Tadahiro, Qiu, Bo, & Yamaguchi, Ryohei. (2021) Observed response of marine boundary layer cloud to the interannual variations of summertime Oyashio extension SST front. Climate Dynamics, 56(11-12), 3511–3526. https://doi.org/10.1007/s00382-021-05649-4

Tian, B., I. M. Held, N.-C. Lau, and B. J. Soden (2005), Diurnal cycle of summertime deep convection over North America: A satellite perspective, J. Geophys. Res., 110, D08108, doi:10.1029/2004JD005275.

Vogel, Raphaela, Nuijens, Louise, & Stevens, Bjorn. (2016) The role of precipitation and spatial organization in the response of trade-wind clouds to warming. Journal of Advances in Modeling Earth Systems, 8(2), 843–862. https://doi.org/10.1002/2015MS000568

Wang, Z. and Sassen, K. (2007) Level 2 cloud scenario classification product process description and interface control document. Ver- sion, 5, 50.

Wilcox, E. M., Harshvardhan, and Platnick, S. (2009) Estimate of the impact of absorbing aerosol over cloud on the MODIS retrievals of cloud optical thickness and effective radius using two independent retrievals of liquid water path, J. Geophys. Res.-Atmos., 114, D05210, https://doi.org/10.1029/2008jd010589.

Winker, D. M., B. H. Hunt, and M. J. McGill (2007) Initial performance assessment of CALIOP, Geophys. Res. Lett., 34, L19803.

Wolanski, E., (1982) Low-Level Trade Winds Over the Western Coral Sea. Journal of Applied Meteorology, 21, 881–882.

Wood, Robert, & Bretherton, Christopher S. (2006) On the Relationship between Stratiform Low Cloud Cover and Lower-Tropospheric Stability. Journal of Climate, 19(24), 6425–6432. https://doi.org/10.1175/JCLI3988.1

Wood, R. and D. L. Hartmann (2006) Spatial variability of liquid water path in marine boundary layer clouds: The importance of mesoscale cellular convection. J. Clim., 19, 1748-1764.

Wood, R., Wyant, M., Bretherton, C. S., Rémillard, J., Kollias, P., Fletcher, J., et al. (2015) Clouds, aerosols, and precipitation in the marine boundary layer: An ARM mobile facility deployment. Bulletin of the American Meteorological Society, 96(3), 419–440. https://doi.org/ 10.1175/BAMS-D-13-00180.1

Yang, G.-Y., and J. M. Slingo (2001), The diurnal cycle in the tropics, Mon. weather Rev., 129, 784-801.

Zhao W., Y. Huang, Steven T. Siems, Michael J. Manton (2021) The role of clouds in coral bleaching events over the Great Barrier Reef, Geophysical Research Letters, doi:10.1029/2021GL093936.

Zhou, X., Kollias, P., & Lewis, E. R. (2015) Clouds, precipitation, and marine boundary layer structure during the MAGIC field campaign. Journal of Climate, 28(6), 2420–2442. https://doi.org/10.1175/JCLI-D-14-00320.1

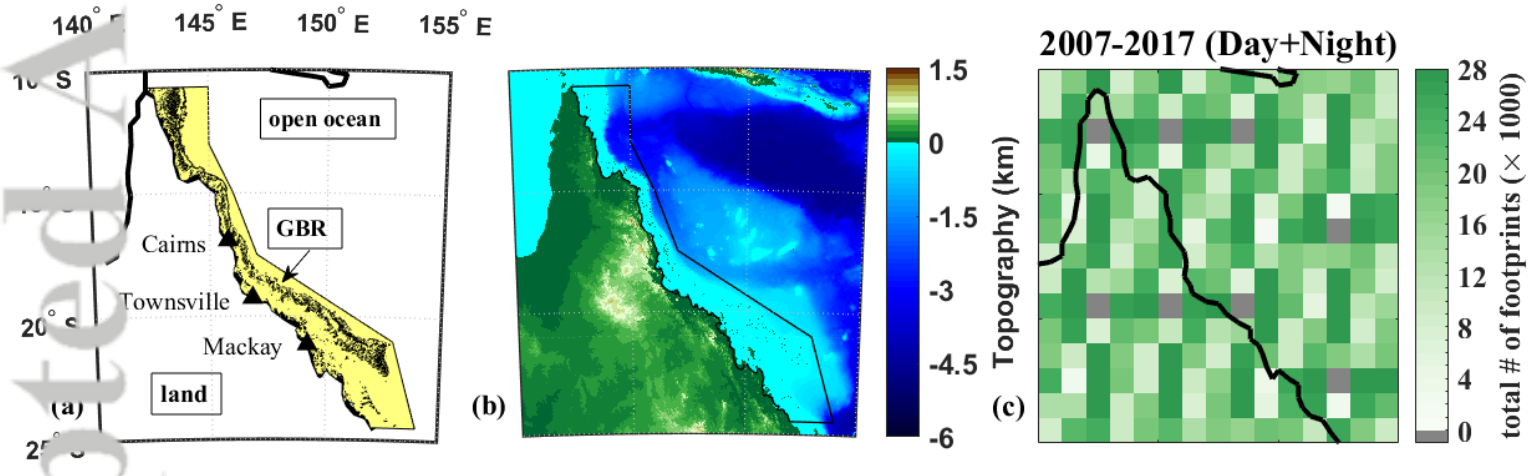

JOC_7660_Figure1_R2_finalversion.tif

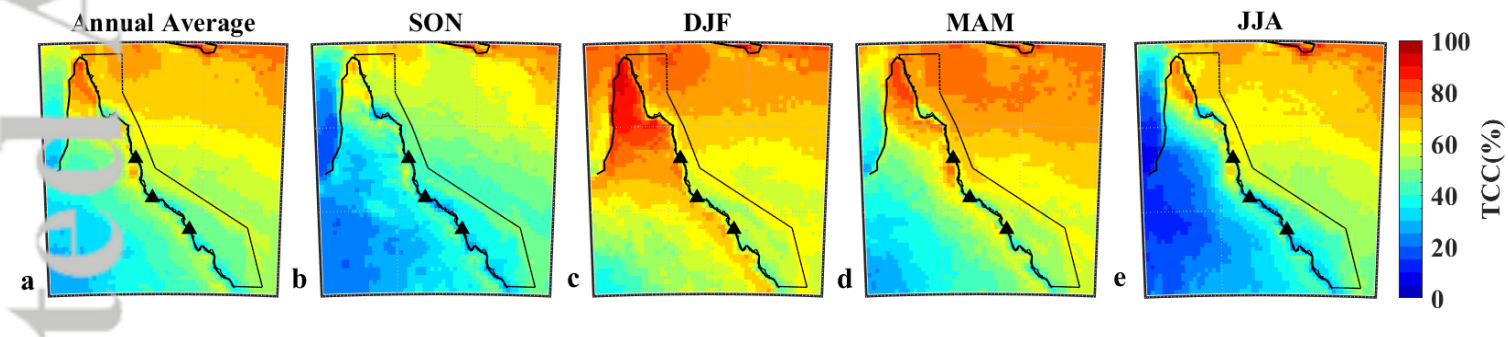

JOC_7660_Figure2_R2_final_version.tif

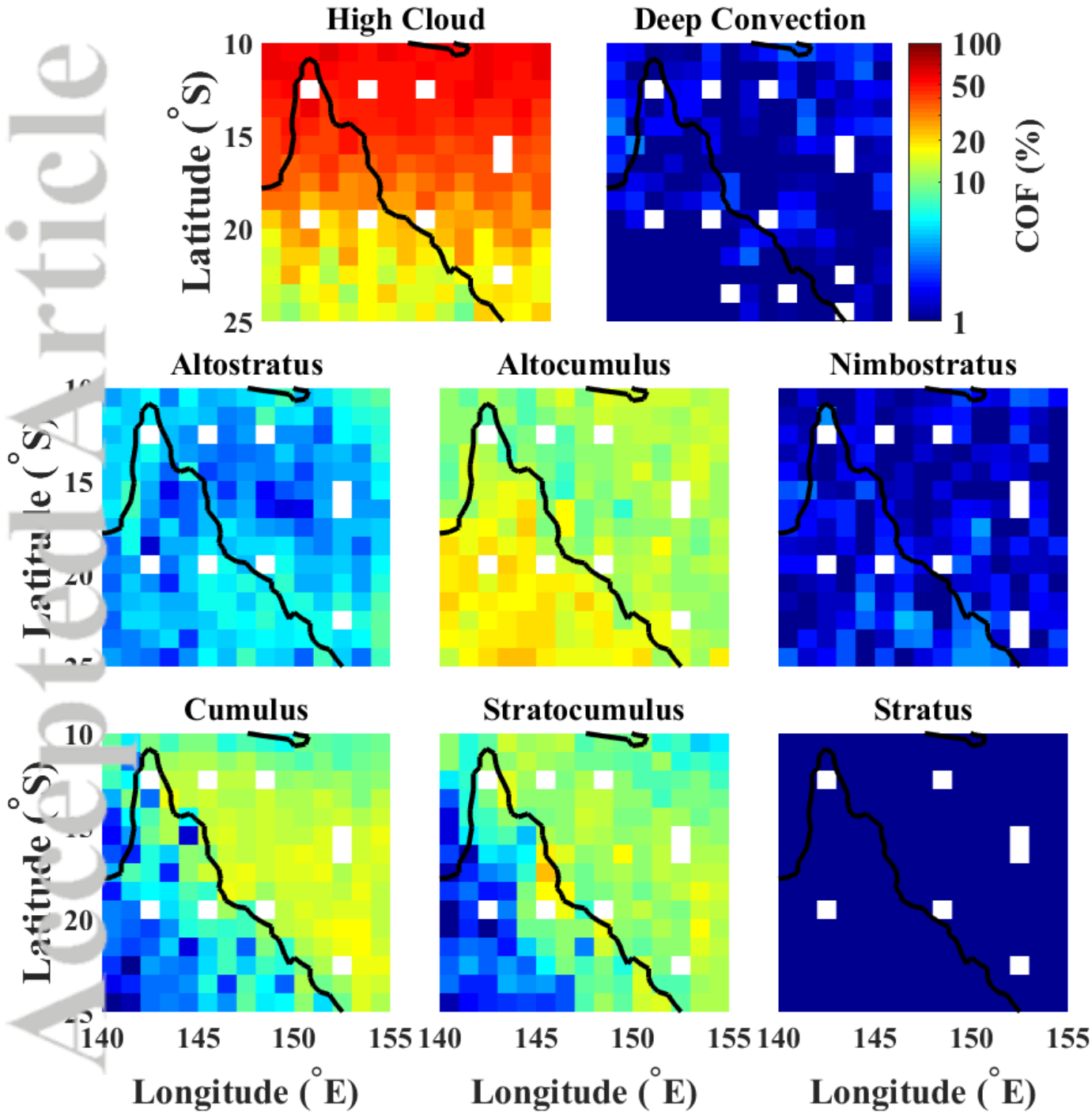

JOC_7660_Figure3_R2_final_version.tif

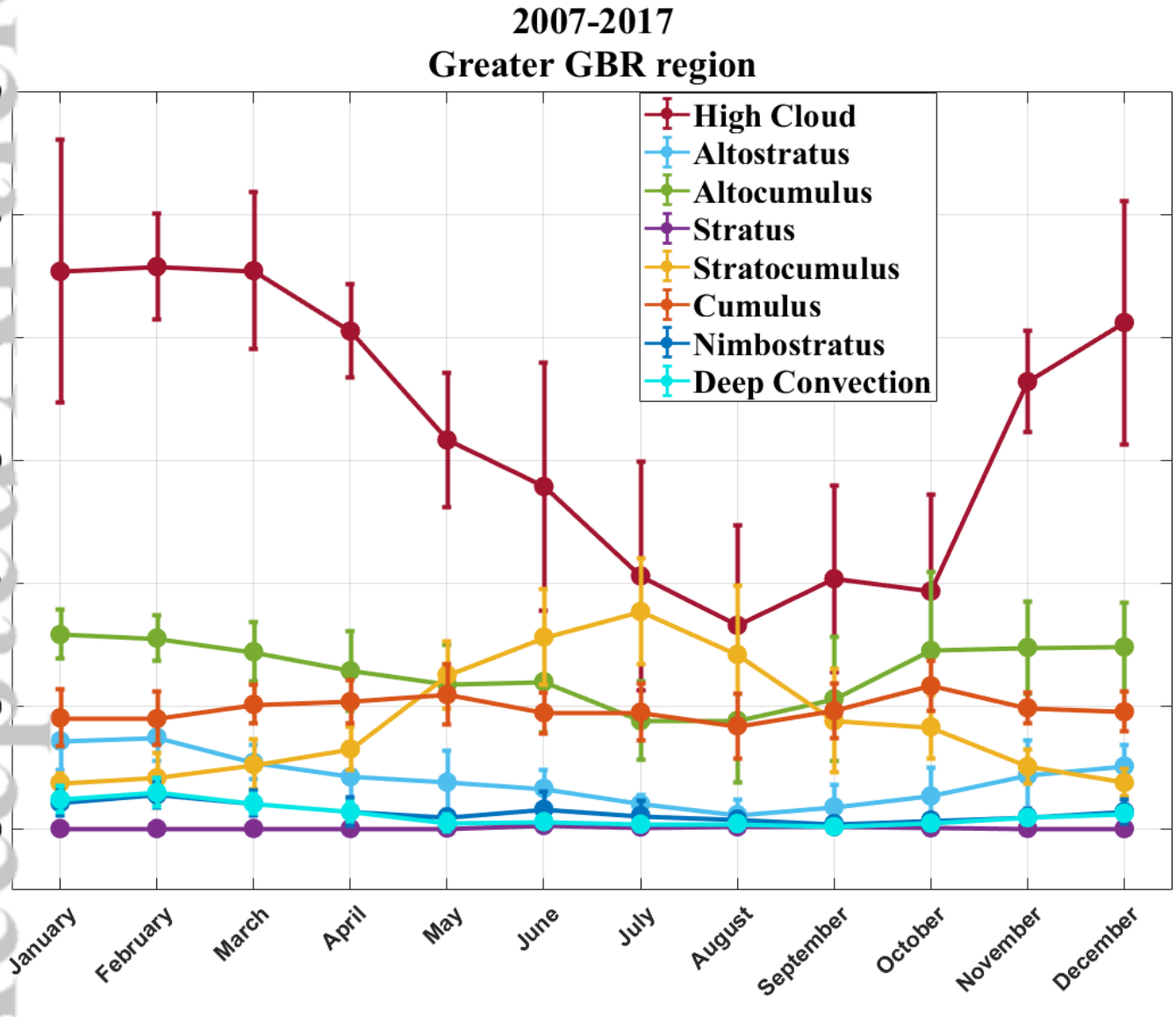

JOC_7660_Figure4_R2_final_version.tif

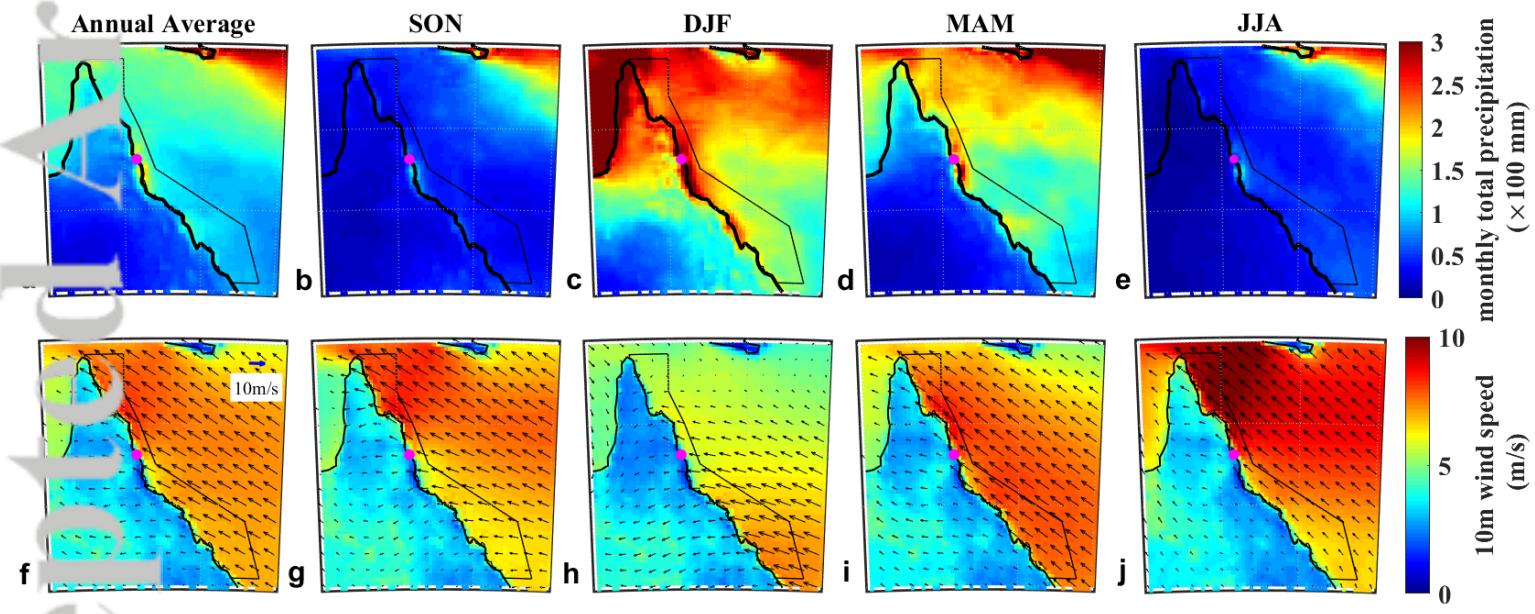

JOC_7660_Figure5_R2_final_version.tif

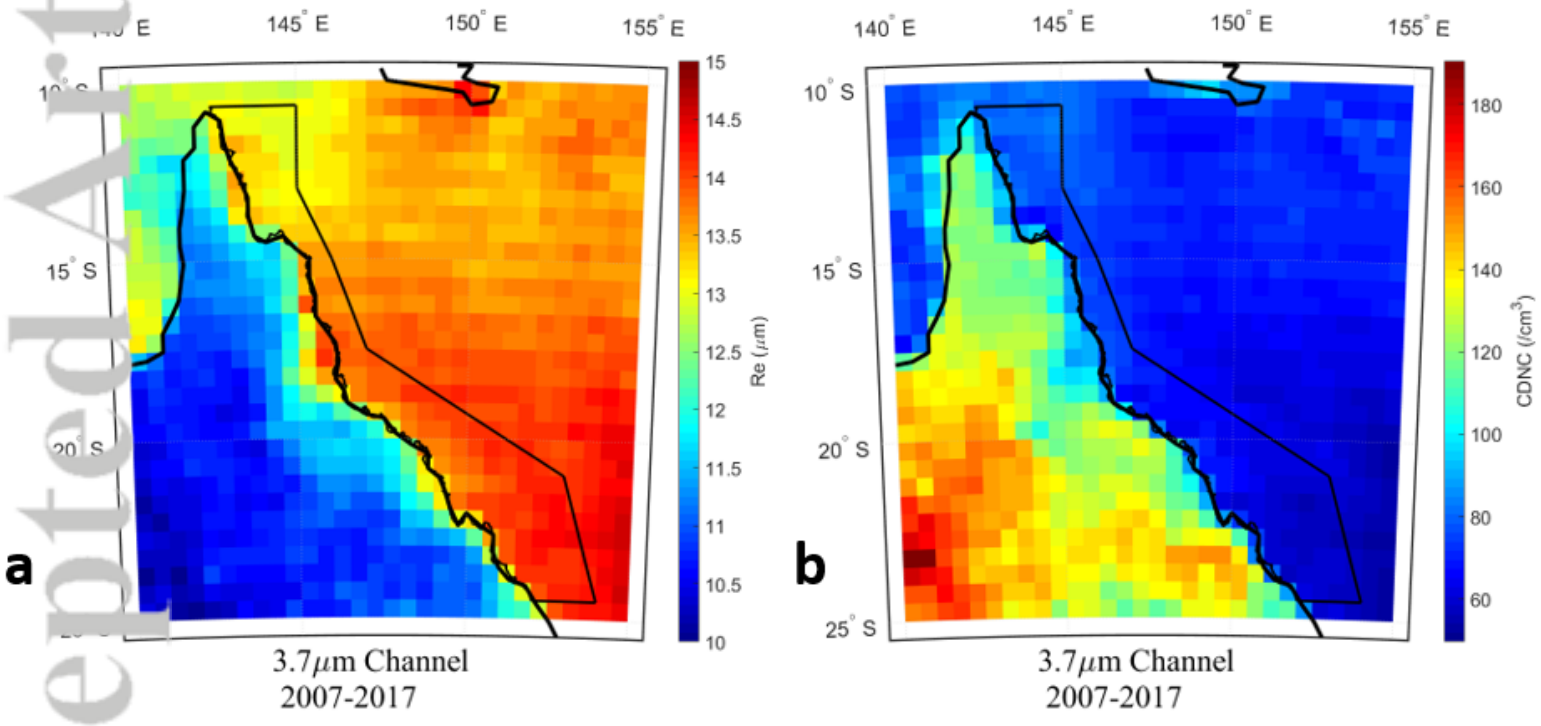

JOC_7660_Figure6_R2_final_version.tif

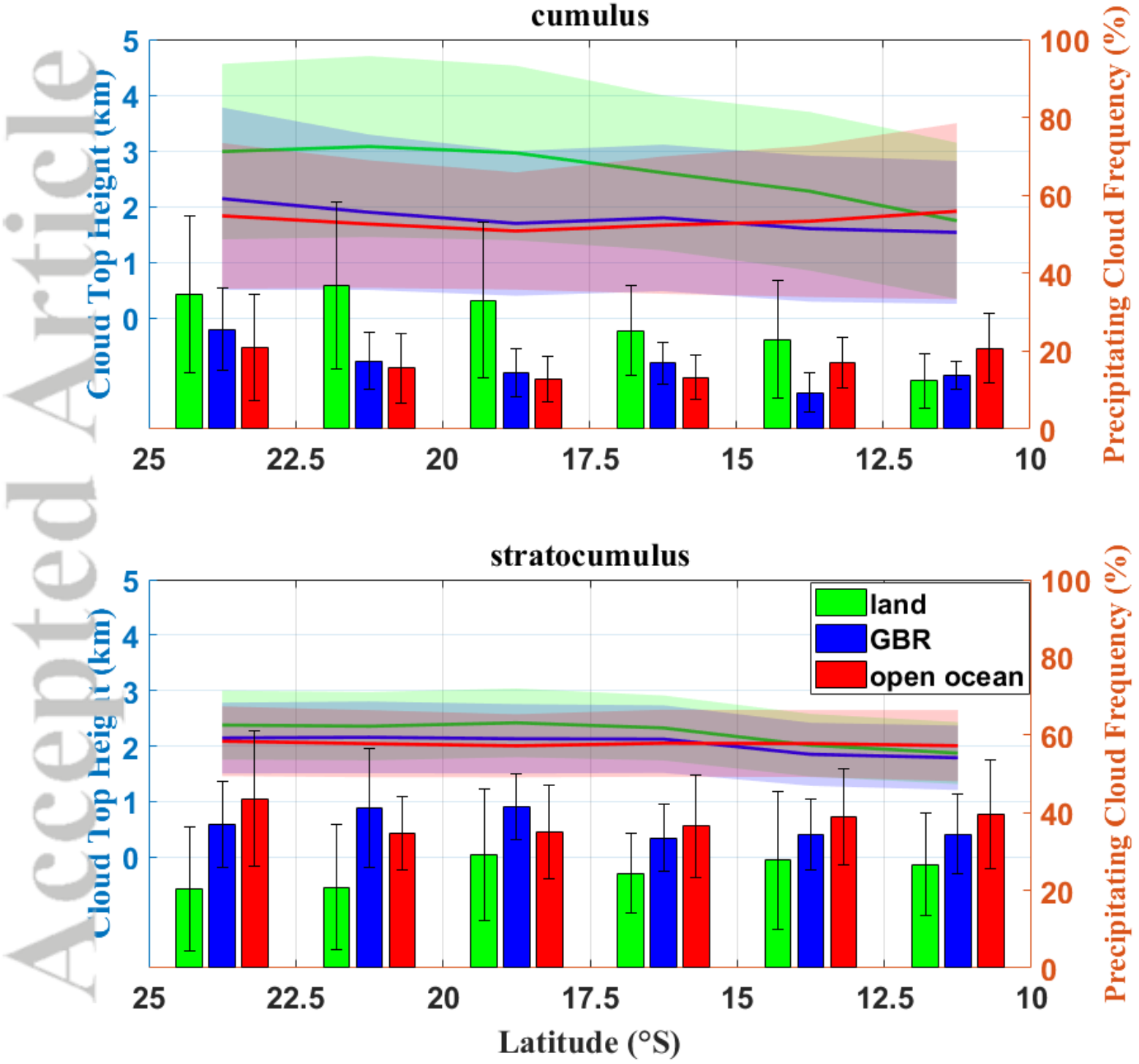

JOC_7660_Figure7_R2_final_version.tif

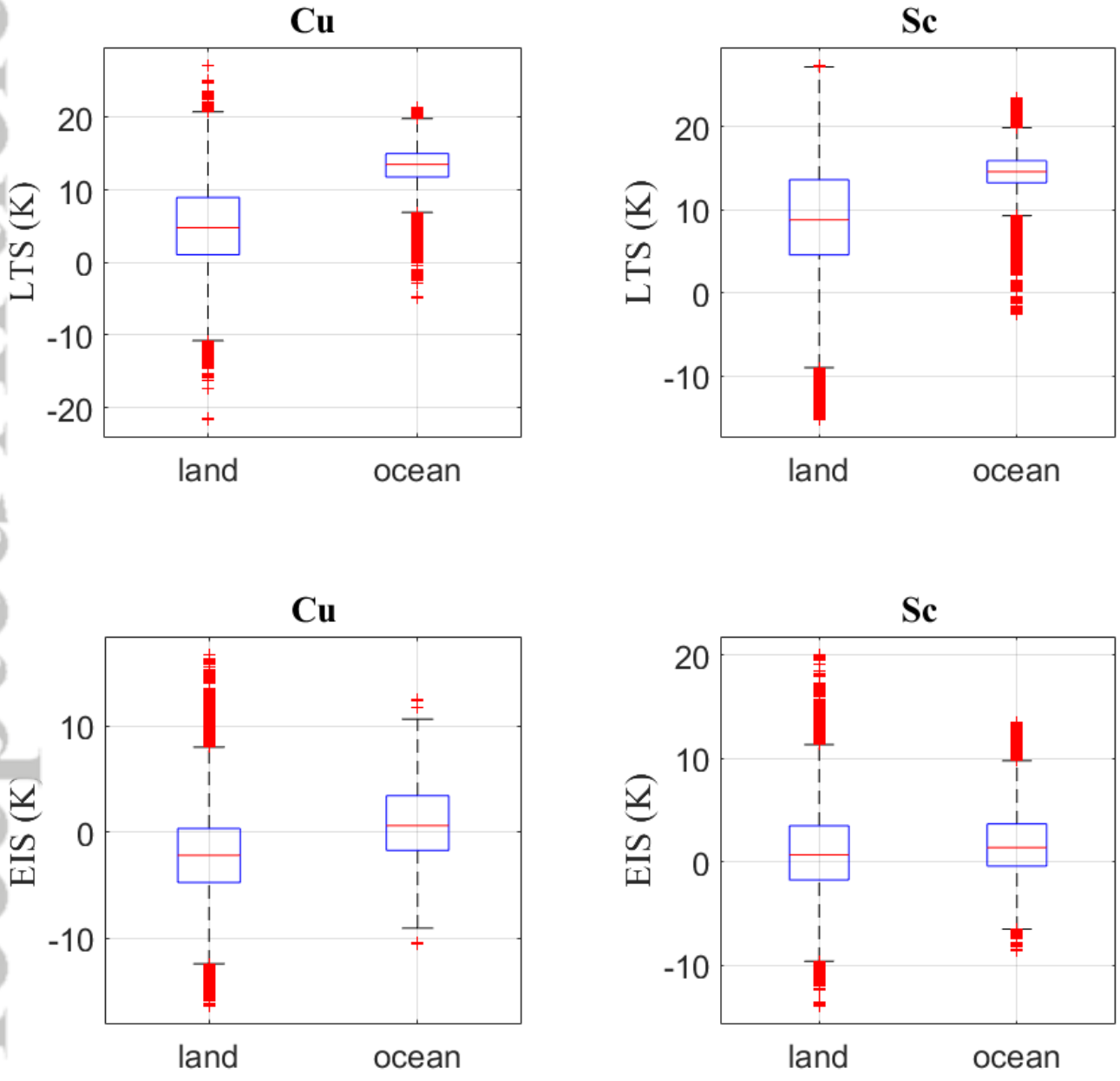

JOC_7660_Figure8_R2_final_version.tif

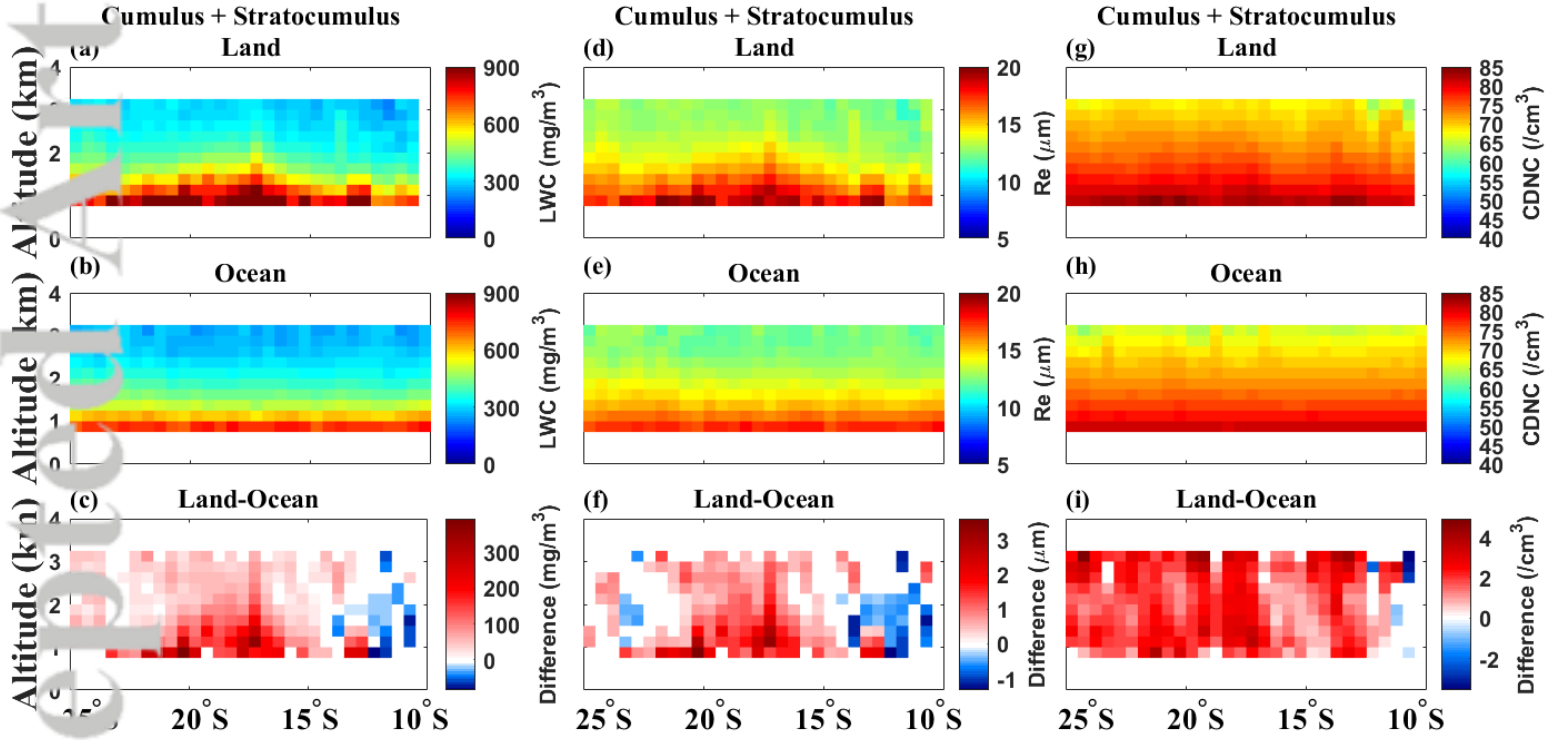

JOC_7660_Figure9_R2_final_version.tif

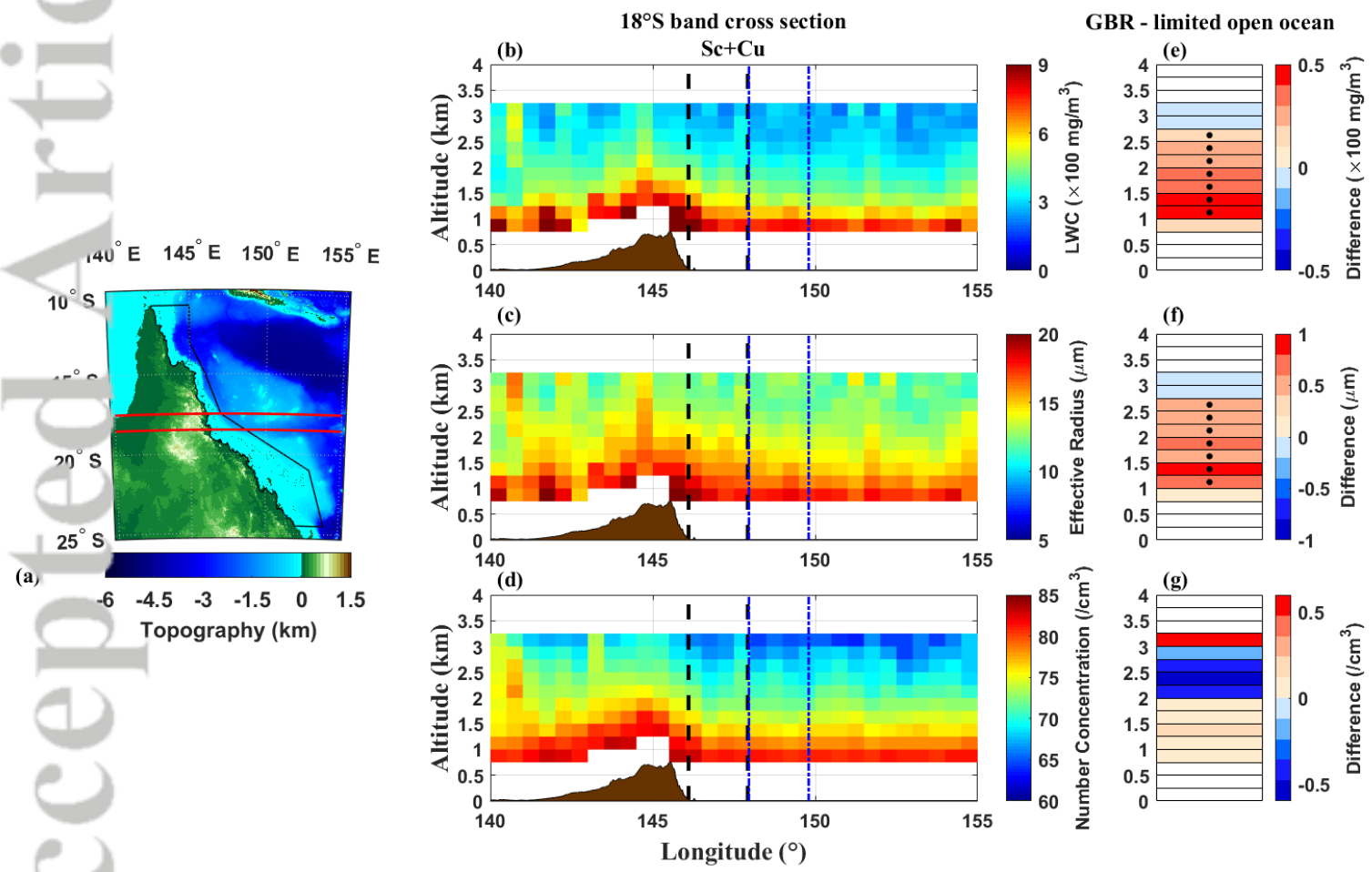

JOC_7660_Figure10_R2_final_version.tif

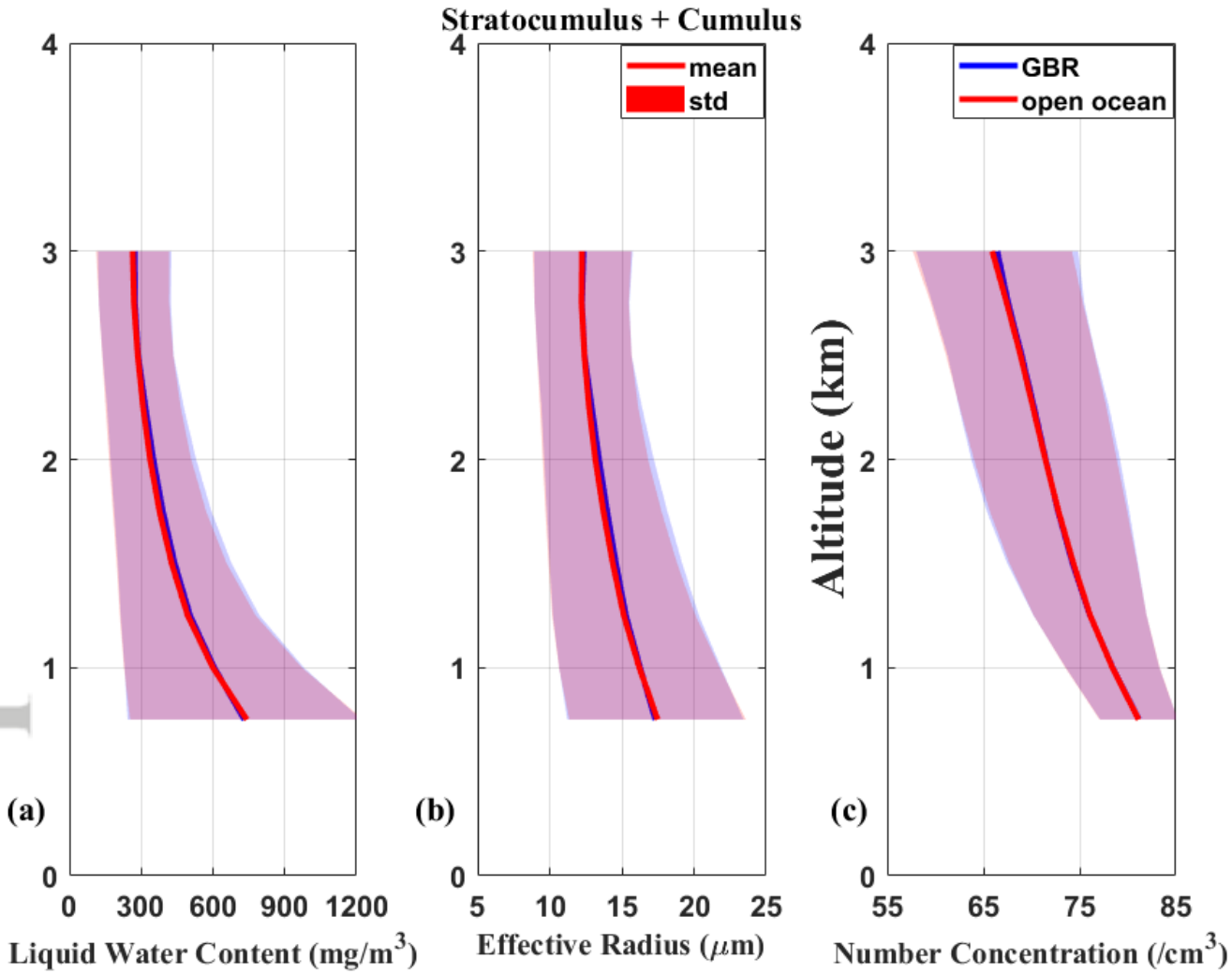

JOC_7660_Figure11_R2_final_version.tif

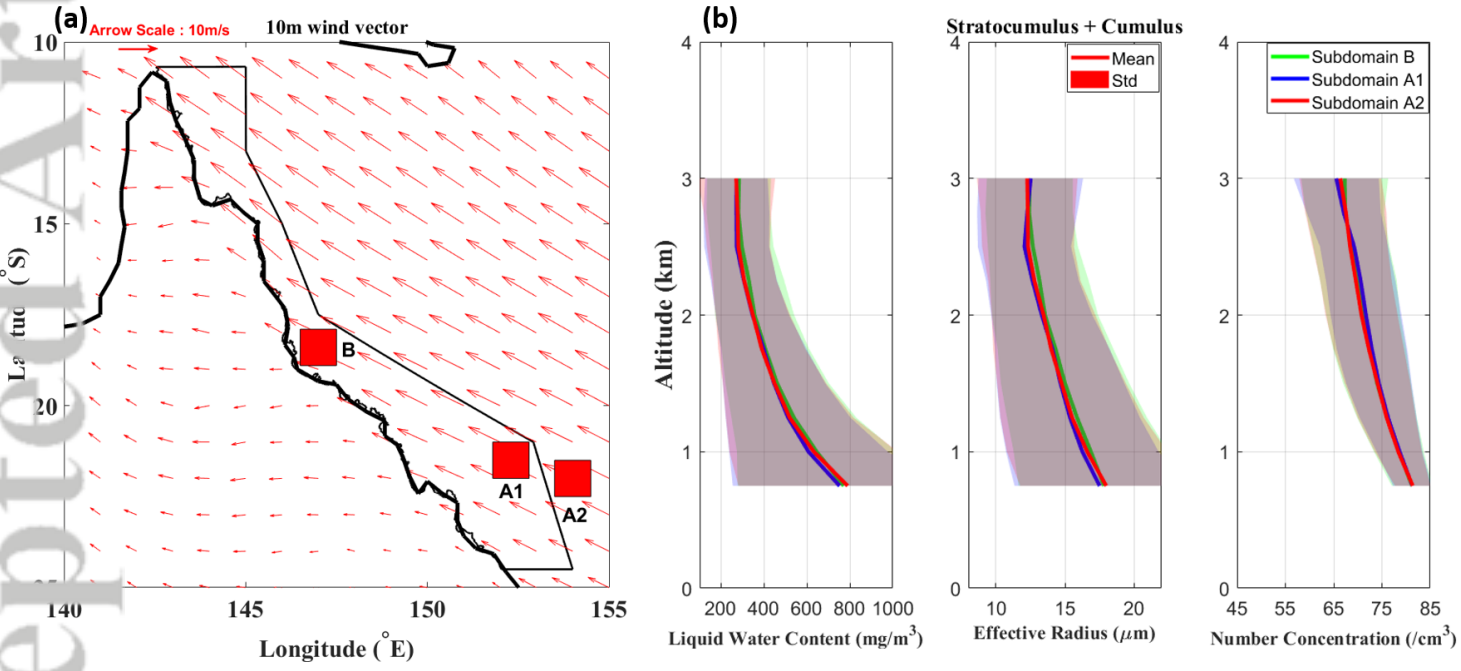

JOC_7660_Figure12_R2_final_version.tif

A characterization of clouds over the Great Barrier Reef and the role of local forcing

Wenhui Zhao*, Yi Huang, Steven Siems, Michael Manton

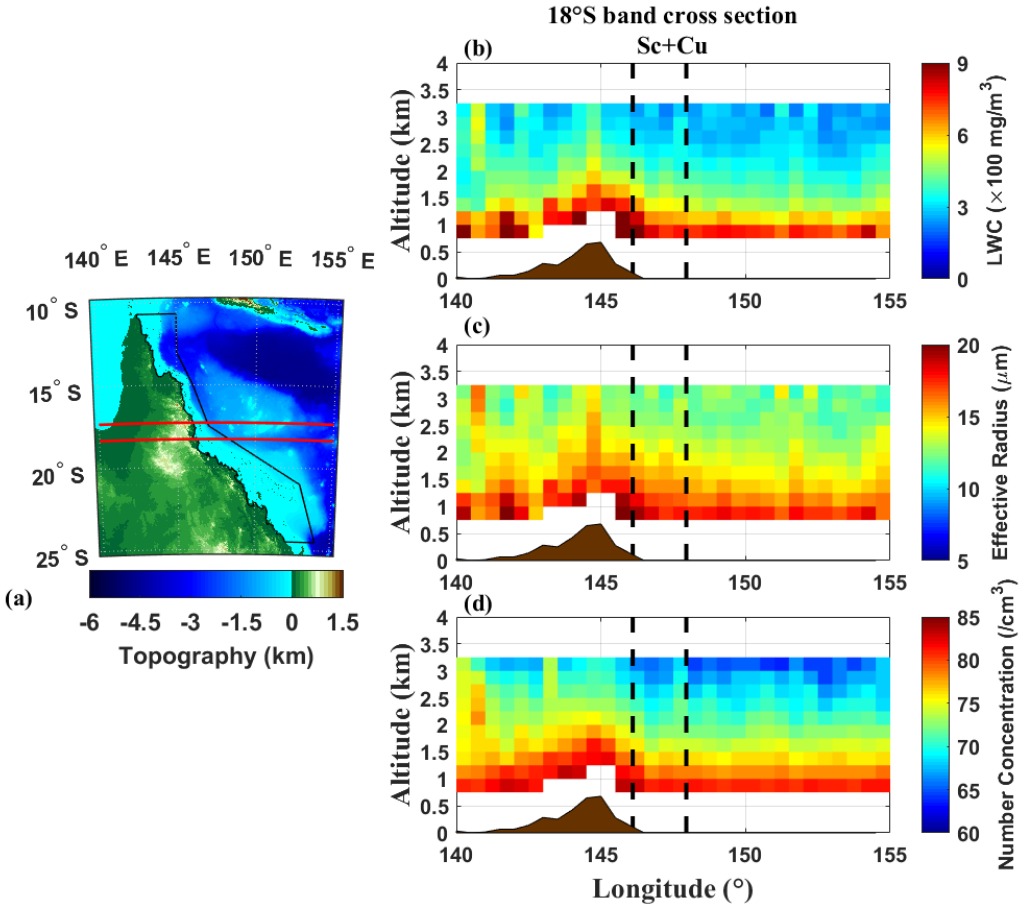

- Different cloud types are observed over different areas of the Greater Barrier Reef region and vary by season;
- Independent satellite observations show good agreement on significant warm cloud properties orography enhancement near Cairns in the wet tropics, with these enhancements extending further east to the coral reef area;
- There is no significant response of low-level clouds to the reef-related microphysical perturbations identified over the Great Barrier Reef region.